TICAM REPORT 97-21
November, 1997

A Discontinuous hp Finite Element Method for Diffusion Problems

J. Tinsley Oden, Ivo Babuska and Carlos Erik Baumann

A DISCONTINUOUS *hp* FINITE ELEMENT METHOD FOR DIFFUSION PROBLEMS

J. Tinsley Oden,[1] Ivo Babuška,[2] and Carlos Erik Baumann[3]

Texas Institute for Computational and Applied Mathematics
The University of Texas at Austin
Austin, Texas 78712

Abstract

We present an extension of the discontinuous Galerkin method (DGM) which is applicable to the numerical solution of diffusion problems. The method involves a weak imposition of continuity conditions on the solution values and on fluxes across interelement boundaries. Within each element, arbitrary spectral approximations can be constructed with different orders p in each element. We demonstrate that the method is elementwise conservative, a property uncharacteristic of high order finite elements.

For clarity, we focus on a model class of linear second-order boundary value problems, and we develop *a priori* error estimates, convergence proofs, and stability estimates. The results of numerical experiments on h- and p-convergence rates for representative two-dimensional problems suggest that the method is robust and capable of delivering exponential rates of convergence.

1 Introduction

This paper presents a new type of discontinuous Galerkin method that is applicable to a broad class of partial differential equations. In particular, this paper addresses the treatment of diffusion operators by finite element techniques in which both the approximate solution and the approximate fluxes can experience discontinuities across interelement boundaries. Among features of the method and aspects of the study presented here are the following:

- *a priori* error estimates are derived so that the parameters affecting the rate of convergence and limitations of the method are established;
- the method is suited for adaptive control of error, and can deliver high-order accuracy where the solution is smooth;
- the method is robust and exhibits elementwise conservative approximations;

[1]Director of TICAM, Cockrell Family Regents Chair in Engineering # 2
[2]Senior Scientist, TICAM, and Robert Trull Chair in Engineering
[3]Research Assistant

- adaptive versions of the method allow for near optimal meshes to be generated; and
- the cost of solution and implementation is acceptable.

The use of discontinuous finite element methods for second- and fourth-order elliptic problems dates back to the early 1960's; when hybrid methods were developed by Pian an his collaborators. The mathematical analysis of hybrid methods was done by Babuška [4], Babuška, Oden, and Lee [6] [7], and others. In 1971, Nitsche [12] introduced the concept of replacing the boundary multipliers with the normal fluxes, and added stabilization terms to produce optimal convergence rates. Similar approaches can be traced back to the work of Percell and Wheeler [14], Wheeler [15], and Arnold [1]. A different approach was the $p-$formulation of Delves and Hall [10], they developed the so-called Global Element Method (GEM); applications of the latter were presented by Hendry and Delves in [11]. The GEM consists essentially in the classical hybrid formulation for a Poisson problem with the Lagrange multiplier eliminated in terms of the dependent variables; namely, the Lagrange multiplier is replaced by the average flux across interelement boundaries. A major disadvantage of the GEM is that the matrix associated with space discretizations of diffusion operators is indefinite, thus the method is unable to solve time dependent diffusion problems; and being indefinite, the linear systems associated with steady state diffusion problems needs special iterative schemes. Moreover, the conditions under which the method is stable and convergent are not known. The interior penalty formulations of Wheeler [15] and Arnold [1] utilize the bilinear form of the GEM augmented with a penalty term which includes the jumps of the solution across elements. The disadvantages of the last approach include the dependence of stability and convergence rates on the penalty parameter, the loss of the conservation property at element level, and a bad conditioning of the matrices. The DGM for diffusion operators developed in this study is a modification of the GEM, which is free of the above deficiencies. More details on these formulations, and the relative merits of each one will be presented in Section 3.1.

In the present investigation, a discontinuous Galerkin method for second-order systems of partial differential equations is presented in which the solution and its derivatives are discontinuous across element boundaries. The resulting scheme is elementwise conservative, a property not common to finite element methods, particularly high-order methods. The formulation supports *h-, p-, and hp*-version approximations and can produce sequences of approximate solutions that are exponentially convergent in standard norms. We explore the stability of the method for one- and two-dimensional model problems and we present *a priori* error estimates. Optimal order h- and p-convergence in the H^1 norm is observed in one- and two-dimensional applications.

Following this introduction, various mathematical preliminaries and notations are presented in Section 2. Section 3 presents a variational formulation of a general linear diffusion problem in a functional setting that admits discontinuities in fluxes and values of the solution across subdomains. Here properties of this weak formulation are presented, laying the groundwork for discontinuous Galerkin approximations that are taken up in Section 4. In Section 4, the discontinuous Galerkin method for diffusion problems is presented. A study of the stability

of the method is presented and *a priori* error estimates are derived. These theoretical results are then confirmed with numerical experiments. The results of several applications of the method to two-dimensional model problems are recorded and discussed. It is shown, among other features, that exponential rates of convergence can be attained.

2 Preliminaries and Notations

2.1 Model Problems

Our goal in this investigation is to develop and analyze one of the main components of a new family of computational methods for a broad class of flow simulations. In this paper we analyze the diffusion operator, model problems in this class are those characterizing diffusion phenomena of a scalar-valued field u, the classical equation governing such steady-state phenomena in a bounded Lipschitz domain $\Omega \subset I\!R^d$, $d = 1, 2,$ or 3, is:

$$\boxed{-\boldsymbol{\nabla}\cdot(\boldsymbol{A}\boldsymbol{\nabla}u) = S \quad \text{in } \Omega} \tag{1}$$

where $S \in L^2(\Omega)$, and $\boldsymbol{A} \in (L^\infty(\Omega))^{d\times d}$ is a diffusivity matrix characterized as follows:

$$\begin{gathered}\boldsymbol{A}(\boldsymbol{x}) = \boldsymbol{A}^T(\boldsymbol{x}), \\ \alpha_1 \boldsymbol{a}^T\boldsymbol{a} \geq \boldsymbol{a}^T\boldsymbol{A}(\boldsymbol{x})\boldsymbol{a} \geq \alpha_0 \boldsymbol{a}^T\boldsymbol{a}, \quad \alpha_1 \geq \alpha_0 > 0, \quad \forall \boldsymbol{a} \in I\!R^d,\end{gathered} \tag{2}$$

a.e. $\boldsymbol{x}$ in Ω.

The boundary $\partial\Omega$ consists of two disjoint parts, Γ_{D} on which Dirichlet conditions are imposed, and Γ_{N} on which Neumann conditions are imposed: $\Gamma_{\mathrm{D}} \cap \Gamma_{\mathrm{N}} = \emptyset$, $\Gamma_{\mathrm{D}} \cup \Gamma_{\mathrm{N}} = \partial\Omega$, and *meas* $\Gamma_{\mathrm{D}} > 0$. whereas boundary conditions are

$$\boxed{\begin{aligned} u &= f \quad \text{on } \Gamma_{\mathrm{D}} \\ (\boldsymbol{A}\boldsymbol{\nabla}u)\cdot\boldsymbol{n} &= g \quad \text{on } \Gamma_{\mathrm{N}} \end{aligned}} \tag{3}$$

Unfortunately, the classical statement (1)-(2) of these model problems rarely makes sense from a mathematical point of view. In realistic domains Ω and for general data $(\boldsymbol{A}, S, f, g)$, the regularity of the solution u may be too low to allow a pointwise interpretation of the solution of these equations. For this reason, weak forms of the model problem must be considered in an appropriate functional setting.

2.2 Functional settings

As noted previously, $\Omega \subset \mathbb{R}^d$, $d = 1, 2$, or 3, denotes a bounded Lipschitz domain. For classes of functions defined on Ω, we shall employ standard Sobolev space notations; thus, $H^m(\Omega)$ is the Hilbert space of functions defined on Ω with generalized derivatives of order $\leq m$ in $L^2(\Omega)$. The standard norm on $H^m(\Omega)$ is denoted $\|u\|_{H^m(\Omega)}$ or simply $\|u\|_m$, and the seminorm on $H^m(\Omega)$ is denoted $|u|_m$. Spaces $H^s(\Omega)$, for $s > 0$ not an integer, are defined by interpolation. The closure of $C_0^\infty(\Omega)$ in $H^m(\Omega)$ is $H_0^m(\Omega)$, and $H^{-m}(\Omega)$ denotes the dual of $H_0^m(\Omega)$.

2.3 Standard weak formulation and Galerkin approximation

A classical weak formulation of problem (1-3) is stated as follows:

$$\boxed{\begin{array}{l}\text{Find } u \in V(\Omega) \text{ such that} \\ \qquad B(u,v) = L(v) \quad \forall\, v \in V(\Omega)\end{array}} \tag{4}$$

where

$$V(\Omega) = \left\{ v \in H^1(\Omega) : \gamma_0 v|_{\Gamma_D} = 0 \right\},$$

$$B(u,v) = \int_\Omega \boldsymbol{\nabla} v \cdot \boldsymbol{A}\, \boldsymbol{\nabla} u \, \mathrm{d}\mathbf{x}, \qquad L(v) = \int_\Omega vS \, \mathrm{d}\mathbf{x} + \int_{\Gamma_N} v\, g \, \mathrm{ds} - B(\overline{u}, v),$$

and $\overline{u} \in H^1(\Omega)$ is such that $\gamma_0 \overline{u}|_{\Gamma_D} = f$, γ_0 being the trace operator. A weak solution of problem (1-3) is $u + \overline{u}$.

The existence of solutions to (4) can be established using the classical Generalized Lax-Milgram theorem.

THEOREM 2.1 *Let $\mathcal{H}$ and $\mathcal{G}$ be Hilbert spaces, and $B : \mathcal{H} \times \mathcal{G} \longrightarrow \mathbb{R}$ a bilinear functional with the following three properties:*

i. There exist a constant $M > 0$ such that

$$B(u,v) \leq M \|u\|_{\mathcal{H}} \|v\|_{\mathcal{G}}, \quad \forall u \in \mathcal{H}, v \in \mathcal{G},$$

where $\|.\|_{\mathcal{H}}$ and $\|.\|_{\mathcal{G}}$ denote the norms on $\mathcal{H}$ and $\mathcal{G}$, respectively.

ii. There exist a constant $\gamma > 0$ such that

$$\inf_{\substack{u \in \mathcal{H} \\ \|u\|_{\mathcal{H}} = 1}} \sup_{\substack{v \in \mathcal{G} \\ \|v\|_{\mathcal{G}} \leq 1}} |B(u,v)| \geq \gamma,$$

iii. And

$$\sup_{u \in \mathcal{H}} |B(u,v)| > 0, \quad v \neq 0, \quad v \in \mathcal{G}.$$

Let L be a continuous linear functional on $\mathcal{G}$. Then there exist a unique solution to the following problem:

Find $u \in \mathcal{H}$ such that

$$B(u,v) = L(v) \quad \forall v \in \mathcal{G}. \tag{5}$$

Moreover,

$$\|u\|_{\mathcal{H}} \leq \frac{1}{\gamma} \|L\|_{\mathcal{G}'}.$$

■

A Galerkin approximation of (5) consists of constructing families of closed (generally finite dimensional) subspaces, $\mathcal{H}_h \subset \mathcal{H}$, $\mathcal{G}_h \subset \mathcal{G}$, and seeking solutions $u_h \in \mathcal{H}_h$ to the following problems:

Find $u_h \in \mathcal{H}_h$ such that

$$B(u_h, v_h) = L(v_h) \quad \forall v_h \in \mathcal{G}_h. \tag{6}$$

Let us assume that the conditions of Theorem 2.1 hold for problem (5), and that (6) is a Galerkin approximation to (5). Then, $B(.,.)$ and $L(.)$ are also continuous on $\mathcal{H}_h \times \mathcal{G}_h$ and $\mathcal{G}_h$, respectively. It follows that (6) is solvable if there exist $\gamma_h > 0$ such that

$$\inf_{\substack{u \in \mathcal{H}_h \\ \|u\|_{\mathcal{H}_h} = 1}} \sup_{\substack{v \in \mathcal{G}_h \\ \|v\|_{\mathcal{G}_h} \leq 1}} |B(u,v)| \geq \gamma_h, \tag{7}$$

and

$$\sup_{u \in \mathcal{H}_h} |B(u,v)| > 0, \quad v \neq 0, \quad v \in \mathcal{G}. \tag{8}$$

A straightforward calculation reveals that the error $u - u_h$ in the approximation (6) of (5) satisfies the estimate

$$\|u - u_h\|_{\mathcal{H}} \leq \left(1 + \frac{M}{\gamma_h}\right) \inf_{w \in \mathcal{H}_h} \|u - w\|_{\mathcal{H}}. \tag{9}$$

Proofs of Theorem 2.1 and of the estimate (9) can be found in [2] and [13].

2.4 Families of regular partitions

Since our discontinuous approximations are to be ultimately defined on partitions of the domain Ω, we now establish notations and conventions for families of regular partitions.

Let $\mathcal{P} = \{\mathcal{P}_h(\Omega)\}_{h>0}$ be a family of regular partitions of $\Omega \subset I\!R^d$ into $N \doteq N(\mathcal{P}_h)$ subdomains Ω_e (see Fig. 1), such that for $\mathcal{P}_h \in \mathcal{P}$,

$$\overline{\Omega} = \bigcup_{e=1}^{N(\mathcal{P}_h)} \overline{\Omega}_e, \quad \text{and } \Omega_e \cap \Omega_f = \emptyset \quad \text{for } e \neq f. \tag{10}$$

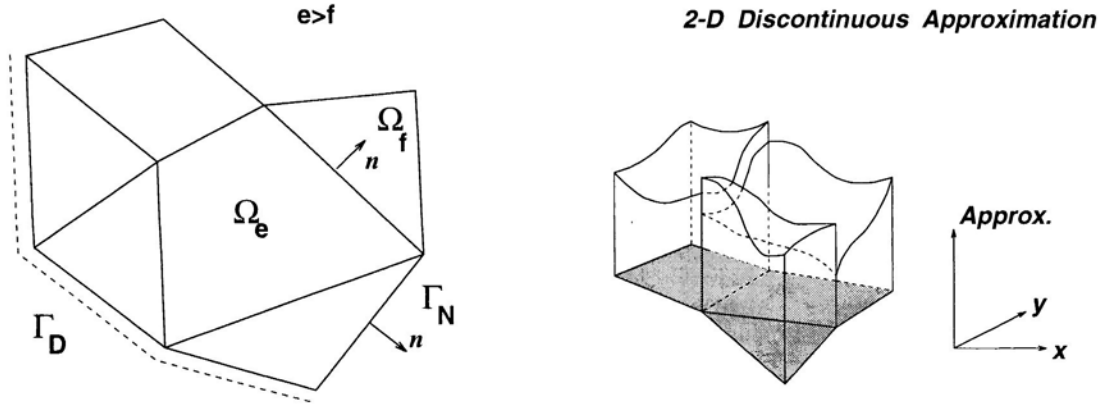

Figure 1: Notation: subdomains and boundaries after discretization.

The partitions $\mathcal{P}_h(\Omega)$ are regular in the sense that if $h_e = \text{diam}(\Omega_e)$, and $\rho_e = \sup\{\text{diam}(\boldsymbol{s}) : \text{sphere } \boldsymbol{s} \subset \Omega_e\}$, then for simplices

$$\frac{h_e}{\rho_e} \leq C \quad 1 \leq e \leq N(\mathcal{P}_h), \tag{11}$$

for every $\mathcal{P}_h(\Omega)$, and for quadrilaterals/hexahedra, if $\hat{h}_e$ =min{lengths of edges of $\partial\Omega_e$}, α_e = min{ interior angles between intersecting edges/faces of $\partial\Omega_e$}, then

$$\frac{h_e}{\hat{h}_e} \leq C, \quad \cos(\alpha_e) < 1, \quad 1 \leq e \leq N(\mathcal{P}_h). \tag{12}$$

for every $\mathcal{P}_h(\Omega)$.

Each subdomain Ω_e has a Lipschitzian boundary $\partial\Omega_e$, which consist of piecewise smooth arcs plus vertices for $d = 2$, and piecewise smooth surfaces and edges for $d = 3$.

Let us define the *interelement boundary* by

$$\Gamma_{\text{int}} = \bigcup_{\Omega_f, \Omega_e \in \mathcal{P}_h} (\partial\Omega_f \cap \partial\Omega_e). \tag{13}$$

On Γ_{int}, we define $\boldsymbol{n} = \boldsymbol{n}_e$ on $(\partial\Omega_e \cap \partial\Omega_f) \subset \Gamma_{\text{int}}$ for indices e, f such that $e > f$.

2.5 Broken spaces

We define the so-called *broken spaces* on the partition $\mathcal{P}_h(\Omega)$:

$$H^m(\mathcal{P}_h) = \left\{ v \in L^2(\Omega) \ : \ v|_{\Omega_e} \in H^m(\Omega_e) \ \ \forall\, \Omega_e \in \mathcal{P}_h(\Omega) \right\}, \tag{14}$$

whe observe that if $v \in H^m(\Omega_e)$, the extension of v to the boundary $\partial\Omega_e$, indicated by the trace operation $\gamma_0 v$, is such that $\gamma_0 v \ \in H^{m-1/2}(\partial\Omega_e)$, $m > 1/2$. The trace of the normal derivative $\gamma_1 v \in H^{m-3/2}(\partial\Omega_e)$, $m > 3/2$, which will be written as $\boldsymbol{\nabla} v \cdot \boldsymbol{n}|_{\partial\Omega_e}$, is interpreted as a generalized flux at the element boundary $\partial\Omega_e$.

With this notation, for $v|_{\Omega_e} \in H^{3/2+\epsilon}(\Omega_e)$ and $v|_{\Omega_f} \in H^{3/2+\epsilon}(\Omega_f)$, we introduce the *jump* operator [.] defined on $\Gamma_{ef} = \overline{\Omega}_e \cap \overline{\Omega}_f \neq \emptyset$ as follows:

$$[\gamma_0 v] = (\gamma_0 v)|_{\partial\Omega_e \cap \Gamma_{ef}} - (\gamma_0 v)|_{\partial\Omega_f \cap \Gamma_{ef}}, \quad e > f, \tag{15}$$

and the *average* operator $\langle . \rangle$ for the normal flux is defined for $(\boldsymbol{A}\boldsymbol{\nabla} v) \cdot \boldsymbol{n} \in L^2(\Gamma_{ef})$, as

$$\langle (\boldsymbol{A}\boldsymbol{\nabla} v) \cdot \boldsymbol{n} \rangle = \frac{1}{2} \left(((\boldsymbol{A}\boldsymbol{\nabla} v) \cdot \boldsymbol{n})|_{\partial\Omega_e \cap \Gamma_{ef}} + ((\boldsymbol{A}\boldsymbol{\nabla} v) \cdot \boldsymbol{n})|_{\partial\Omega_f \cap \Gamma_{ef}} \right), \quad e > f, \tag{16}$$

where $\boldsymbol{A}$ is the diffusivity. Note that $\boldsymbol{n}$ represents the outward normal from the element with higher index.

2.6 Polynomial approximations on partitions

For future reference, we record a local approximation property of polynomial finite element approximations. Let $\hat{\Omega}$ be a regular master element in $\mathbb{R}^d$; e.g. $\hat{\Omega} = (-1,1)^d$. And let $\{F_{\Omega_e}\}$ be a family of invertible maps from $\hat{\Omega}$ onto Ω_e (see Fig. 2).

For every element $\Omega_e \in \mathcal{P}_h$, the finite-dimensional space of real-valued shape functions $\hat{P} \subset H^m\left(\hat{\Omega}\right)$ is taken to be the space $P_{p_e}\left(\hat{\Omega}\right)$ of polynomials of degree $\leq p_e$ defined on $\hat{\Omega}$. Then we define

$$P_{p_e}(\Omega_e) = \left\{\psi \mid \psi = \hat{\psi} \circ F_{\Omega_e}^{-1},\ \hat{\psi} \in \hat{P} = P_{p_e}\left(\hat{\Omega}\right)\right\}. \tag{17}$$

Using the spaces $P_{p_e}(\Omega_e)$, we can define

$$V_p(\mathcal{P}_h) = \prod_{e=1}^{N(\mathcal{P}_h)} P_{p_e}(\Omega_e), \tag{18}$$

$N(\mathcal{P}_h)$ being the number of elements in partition $\mathcal{P}_h$.

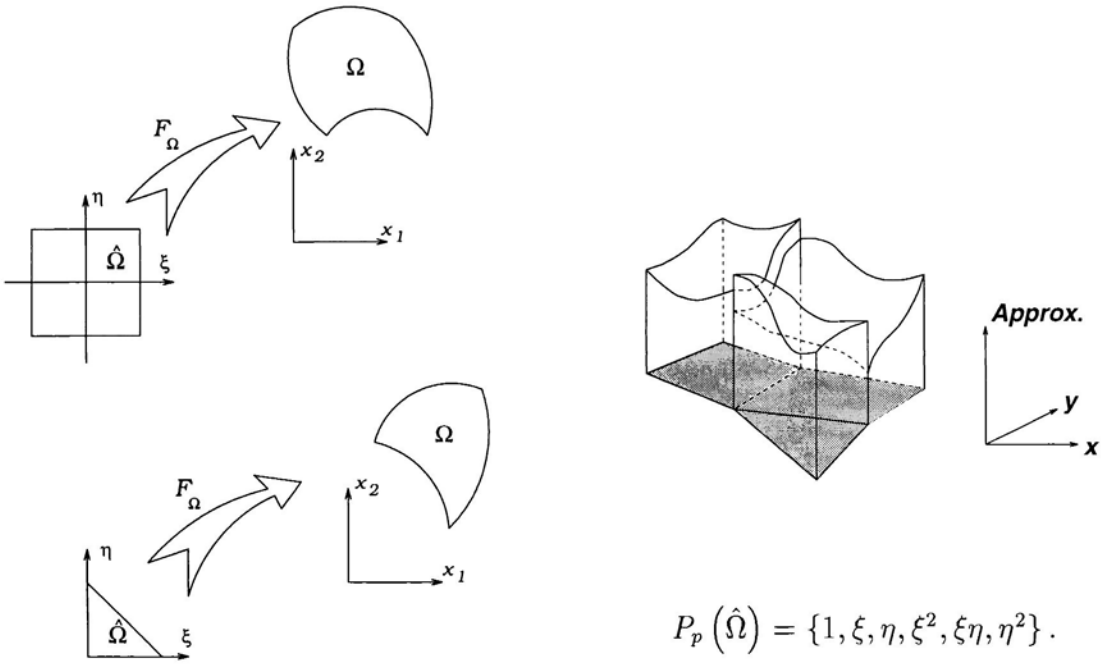

Figure 2: Mappings $\hat{\Omega} \longrightarrow \Omega_e$ and discontinuous approximation.

The approximation properties of $V_p(\mathcal{P}_h)$ will be estimated using standard local approximation estimates (see [3]). Let $u \in H^s(\Omega_e)$; there exist a constant C depending on s and on

the conditions (11) and (12), but independent of u, $h_e = diam(\Omega_e)$, and p_e, and a polynomial u_p of degree p_e, such that for any $0 \leq r \leq s$ the following estimate hold:

$$\|u - u_p\|_{r,\Omega_e} \leq C \frac{h_e^{\mu-r}}{p_e^{s-r}} \|u\|_{s,\Omega_e}, \quad s \geq 0, \tag{19}$$

where $\|.\|_{r,\Omega_e}$ denotes the usual Sobolev norm, and $\mu = min(p_e + 1, s)$.

The following local inverse inequalities for a generic element Ω_e are valid for $u \in P_{p_e}(\Omega_e)$ and $p_e > 0$ (see [5][9]):

$$|u|^2_{0,\partial\Omega_e} \leq C h_e^{-1} p_e^2 \|u\|^2_{0,\Omega_e}, \qquad \left|\frac{\partial u}{\partial n}\right|^2_{0,\partial\Omega_e} \leq C h_e^{-1} p_e^2 |u|^2_{1,\Omega_e}. \tag{20}$$

3 A weak formulation of diffusion problems in Broken Sobolev spaces

We focus on a model linear diffusion problem in a bounded domain, given data $(\Omega, \partial\Omega, S, f, g)$, we wish to find a function u such that

$$\boxed{\begin{aligned} -\boldsymbol{\nabla}\cdot(\boldsymbol{A}\boldsymbol{\nabla}u) &= S \quad \text{in } \Omega \\ u &= f \quad \text{on } \Gamma_{\mathrm{D}} \\ (\boldsymbol{A}\boldsymbol{\nabla}u)\cdot\boldsymbol{n} &= g \quad \text{on } \Gamma_{\mathrm{N}} \end{aligned}} \tag{21}$$

where $\boldsymbol{A} \in (L^\infty(\Omega))^{d\times d}$ is a diffusivity matrix satisfying the conditions stated in (2).

The weak formulation of (21) that forms the basis of our discontinuous Galerkin method is defined on a broken space $V(\mathcal{P}_h)$, $\mathcal{P}_h$ being a member of a family of regular partitions of Ω. In particular, $V(\mathcal{P}_h)$ is a Hilbert space on the partition $\mathcal{P}_h$, which is the completion of $H^{3/2+\epsilon}(\mathcal{P}_h)$, $\epsilon > 0$, with respect to the following mesh-dependent norm:

$$\|v\|^2_V = |v|^2_{1,\mathcal{P}_h} + |v|^2_{0,\Gamma_{\mathcal{P}_h}}, \tag{22}$$

where

$$|v|^2_{1,\mathcal{P}_h} = \sum_{\Omega_e \in \mathcal{P}_h} \int_{\Omega_e} \boldsymbol{\nabla} v \cdot \boldsymbol{A}\, \boldsymbol{\nabla} v \, \mathrm{dx},$$

$$|v|^2_{0,\Gamma_{\mathcal{P}_h}} = \left|h^{-\alpha}\, \gamma_0 v\right|^2_{0,\Gamma_{\mathrm{D}}} + |h^{\alpha}\, (\boldsymbol{A}\boldsymbol{\nabla}v)\cdot\boldsymbol{n}|^2_{0,\Gamma_{\mathrm{D}}} + \left|h^{-\alpha}\, [\gamma_0 v]\right|^2_{0,\Gamma_{\mathrm{int}}} + |h^{\alpha}\, \langle(\boldsymbol{A}\boldsymbol{\nabla}v)\cdot\boldsymbol{n}\rangle|^2_{0,\Gamma_{\mathrm{int}}}, \tag{23}$$

and

$$|v|^2_{0,\Gamma} = \int_\Gamma v^2 \, \mathrm{ds}, \quad \text{for} \quad \Gamma \in \{\Gamma_{\mathrm{D}}, \Gamma_{\mathrm{N}}, \Gamma_{\mathrm{int}}\}.$$

In (23), the value of h is $h_e/(2\alpha_1)$ on $\Gamma_{\rm D}$, and the average $(h_e+h_f)/(2\alpha_1)$ on that part of $\Gamma_{\rm int}$ shared by two generic elements Ω_e and Ω_f, the constant α_1 being defined in (2). A complete characterization of the space $V(\mathcal{P}_h)$ for the one-dimensional case is described in [9].

We should note that the terms $h^{\pm\alpha}$, with $\alpha = 1/2$, are introduced to minimize the mesh-dependence of an otherwise strongly mesh-dependent norm. The inner product associated with $\|.\|_V$ is the symmetric bilinear form

$$\begin{aligned}(u,v)_V \;:=\; & \sum_{\Omega_e\in\mathcal{P}_h}\int_{\Omega_e} \boldsymbol{\nabla} v\cdot\ \boldsymbol{A}\ \boldsymbol{\nabla} u\ \mathrm{dx} \\ & + \int_{\Gamma_{\rm D}} \left(h^{-2\alpha}\ \gamma_0 v\ \gamma_0 u + h^{2\alpha}\ (\boldsymbol{A}\boldsymbol{\nabla} v)\cdot\boldsymbol{n}\ (\boldsymbol{A}\boldsymbol{\nabla} u)\cdot\boldsymbol{n}\right)\ \mathrm{ds} \\ & + \int_{\Gamma_{\rm int}} \left(h^{2\alpha}\ \langle(\boldsymbol{A}\boldsymbol{\nabla} v)\cdot\boldsymbol{n}\rangle\langle(\boldsymbol{A}\boldsymbol{\nabla} u)\cdot\boldsymbol{n}\rangle + h^{-2\alpha}\ [\gamma_0 v][\gamma_0 u]\right)\ \mathrm{ds}.\end{aligned} \tag{24}$$

Next, we introduce the bilinear form $B : V(\mathcal{P}_h)\times V(\mathcal{P}_h)\longrightarrow I\!R$, defined by

$$\begin{aligned}B(u,v) = & \sum_{\Omega_e\in\mathcal{P}_h}\int_{\Omega_e} \boldsymbol{\nabla} v\cdot\ \boldsymbol{A}\ \boldsymbol{\nabla} u\ \mathrm{dx} + \int_{\Gamma_{\rm D}} \left((\boldsymbol{A}\boldsymbol{\nabla} v)\cdot\boldsymbol{n}\ u - v\,(\boldsymbol{A}\boldsymbol{\nabla} u)\cdot\boldsymbol{n}\right)\ \mathrm{ds} \\ & + \int_{\Gamma_{\rm int}} \left(\langle(\boldsymbol{A}\boldsymbol{\nabla} v)\cdot\boldsymbol{n}\rangle[u] - \langle(\boldsymbol{A}\boldsymbol{\nabla} u)\cdot\boldsymbol{n}\rangle[v]\right)\ \mathrm{ds},\end{aligned} \tag{25}$$

and the linear form $L : V(\mathcal{P}_h)\longrightarrow I\!R$, defined by

$$L(v) = \sum_{\Omega_e\in\mathcal{P}_h}\left\{\int_{\Omega_e} vS\ \mathrm{dx}\right\} + \int_{\Gamma_{\rm D}} (\boldsymbol{A}\boldsymbol{\nabla} v)\cdot\boldsymbol{n} f\ \mathrm{ds} + \int_{\Gamma_{\rm N}} vq\ \mathrm{ds}. \tag{26}$$

In (25), we denote by $\langle(\boldsymbol{A}\boldsymbol{\nabla} v)\cdot\boldsymbol{n}\rangle$ the limits of the sequences of averaged fluxes $\langle(\boldsymbol{A}\boldsymbol{\nabla} v_k)\cdot\boldsymbol{n}\rangle$ on $\Gamma_{\rm int}$. With these conventions and notations in place, we consider the following weak or variational boundary-value problem

$$\boxed{\begin{array}{l}\text{Find}\ \ u\in V(\mathcal{P}_h)\ \ \text{such that} \\ \qquad\qquad B(u,v) = L(v)\quad \forall\, v\in V(\mathcal{P}_h)\end{array}} \tag{27}$$

That (27) indeed corresponds to our model diffusion problem is verified in the following theorem:

THEOREM 3.1 *Suppose S, f, and g are smooth (continuous) and that the solution u to (21) exists and $(\boldsymbol{A}\boldsymbol{\nabla} u)\in H^1(\mathcal{P}_h)$. Then u is a solution of (27). Conversely, any sufficiently smooth solution of (27) is also a solution of (21).*

Proof: This follows from standard arguments and use of Green's formula. For details, see [9]. ■

Remark 3.1 *Let us note that*

$$B(v,v) = \sum_{\Omega_e \in \mathcal{P}_h} \int_{\Omega_e} \boldsymbol{\nabla} v \cdot \boldsymbol{A} \boldsymbol{\nabla} v \, \mathrm{d}\mathbf{x} \geq 0, \qquad \forall \, v \in V(\mathcal{P}_h), \tag{28}$$

the above inequality only indicates that the bilinear form is positive semidefinite. As shown later, the variational formulation is stable, i.e. it has no zero eigenvalues, therefore $B(.,.)$ is positive definite. It is the skew-symmetric part of $B(.,.)$ that renders it positive definite. ■

3.1 The Global Element Method and interior penalty formulations

The Global Element Method (GEM) ([10][11]) consists in the classical hybrid formulation for a Poisson problem with the Lagrange multiplier eliminated in terms of the dependent variables; namely, the Lagrange multiplier is replaced by the average flux across interelement boundaries. The bilinear form associated with the GEM is the following:

$$\begin{aligned} B(u,v) &= \sum_{\Omega_e \in \mathcal{P}_h} \int_{\Omega_e} \boldsymbol{\nabla} v \cdot \boldsymbol{A} \boldsymbol{\nabla} u \, \mathrm{d}\mathbf{x} - \int_{\Gamma_\mathrm{D}} \left((\boldsymbol{A}\boldsymbol{\nabla} v) \cdot \boldsymbol{n} u + v \, (\boldsymbol{A}\boldsymbol{\nabla} u) \cdot \boldsymbol{n} \right) \, \mathrm{ds} \\ &- \int_{\Gamma_\mathrm{int}} \left(\langle (\boldsymbol{A}\boldsymbol{\nabla} v) \cdot \boldsymbol{n} \rangle [u] + \langle (\boldsymbol{A}\boldsymbol{\nabla} u) \cdot \boldsymbol{n} \rangle [v] \right) \, \mathrm{ds}, \end{aligned} \tag{29}$$

a very important disadvantage of this method is that the matrix associated with the above bilinear form is indefinite, which prevents the solution of time-dependent diffusion problems and also the utilization of many iterative schemes for the solution of steady problems. Given that the goal of this investigation is to obtain a solver for convection diffusion equations within the usual CFD settings, it is of paramount importance to generate a numerical technique which can handle these equations using pseudo time-marching schemes. The inability of the GEM to generate systems of equations which are amenable to the aforementioned solution techniques is the main reason for which we are not to using it. Besides this disadvantage, the GEM performs better than the technique that we advocate when the error is measured in the L^2 norm, which is optimal for any p, this is not the case with the technique that we advocate, which looses one order for even powers p when the error is measured in the L^2 norm. The GEM has the advantage of producing symmetric systems of equations, but this advantage is not of interest for convection-diffusion problems, which are intrinsically non-symmetric (non self-adjoint) problems.

The method of Nitsche [12] and the interior penalty formulations of Wheeler [15] and Arnold [1] are very similar, they are based on a bilinear form given by

$$B(u,v) = \sum_{\Omega_e \in \mathcal{P}_h} \int_{\Omega_e} \boldsymbol{\nabla} v \cdot \boldsymbol{A} \boldsymbol{\nabla} u \, \mathrm{d}\mathbf{x}$$

$$- \int_{\Gamma_D} \left((\boldsymbol{A}\boldsymbol{\nabla} v)\cdot\boldsymbol{n} u + v\,(\boldsymbol{A}\boldsymbol{\nabla} u)\cdot\boldsymbol{n} - \sigma v u \right)\, \mathrm{ds} \tag{30}$$

$$- \int_{\Gamma_{\mathrm{int}}} \left(\langle (\boldsymbol{A}\boldsymbol{\nabla} v)\cdot\boldsymbol{n}\rangle [u] + \langle (\boldsymbol{A}\boldsymbol{\nabla} u)\cdot\boldsymbol{n}\rangle [v] - \sigma [v][u] \right)\, \mathrm{ds},$$

where $\sigma = Kh^{-1}$ is the penalty function. The value of K is critical because if it is too small this technique is the same as the GEM, which has the problem of indefinite systems. In our experience, the parameter K is problem dependent and has to be chosen very carefully, otherwise the rate of convergence is not optimal. Other disadvantages include the loss of the conservation property, and a bad conditioning of the matrices. This technique also produces symmetric systems of equations, but as explained above, this in not an advantage for the type of problems that we are planning to solve.

The DGM developed in this study does not present the deficiencies pointed out before, and we believe is much better suited to the solution of CFD problems.

4 The discontinuous Galerkin method for diffusion problems

The variational formulation (27) will now be used as a basis for the construction of discontinuous Galerkin approximations of the model diffusion problem. In the discontinuous Galerkin method, the partitions of the solution domain, on which the problem (21) is posed, are now finite elements, across common boundaries of which the test functions can experience jumps. The Galerkin approximation is thus defined on a subspace $V_p(\mathcal{P}_h)$ of the Hilbert space $V(\mathcal{P}_h)$ introduced in Section 2. Thus, the general setting of the approximation result (9) is applicable, and can be used to derive *a priori* error estimates for the method.

Let us now consider the finite dimensional subspace $V_p(\mathcal{P}_h) \subset V(\mathcal{P}_h)$ defined in Section 2.6 as

$$V_p(\mathcal{P}_h) = \prod_{e=1}^{N(\mathcal{P}_h)} P_{p_e}(\Omega_e)\,. \tag{31}$$

Our discontinuous Galerkin approximation (27) in $V_p(\mathcal{P}_h)$ is:

$$\boxed{\begin{array}{l} \text{Find } u_h \in V_p(\mathcal{P}_h) \text{ such that} \\ \qquad B(u_h, v_h) = L(v_h) \quad \forall\, v_h \in V_p(\mathcal{P}_h) \end{array}} \tag{32}$$

where $B(.,.)$ and $L(.)$ are defined in (25) and (26), respectively.

An immediate observation is that the discrete scheme defined by (32) is conservative. This is the subject of the following paragraph.

4.1 Strong conservation at element level:

A solution is said to be *globally conservative* if the balance of the *species* (the solution u) is satisfied on solution domain as a whole, and *locally conservative* if a partition of the solution domain exist such that the balance is satisfied within each subdomain of this partition.

Considering a generic element $\Omega_e \in \mathcal{P}_h$, when the test function v_h is a piecewise constant (unit) function with local support on element Ω_e, from (32)-(25)-(26) we obtain the following approximation:

$$-\int_{\partial\Omega_e\cap\Gamma_{\rm D}} (\boldsymbol{A}\boldsymbol{\nabla}u_h)\cdot\boldsymbol{n}\ \mathrm{ds} - \int_{\partial\Omega_e\cap\Gamma_{\rm int}} \langle(\boldsymbol{A}\boldsymbol{\nabla}u_h)\cdot\boldsymbol{n}_e\rangle\ \mathrm{ds} = \int_{\Omega_e} S\ \mathrm{dx} + \int_{\partial\Omega_e\cap\Gamma_{\rm N}} g\ \mathrm{ds}, \quad (33)$$

which means that conservation at element level is insured when the flux across $\partial\Omega_e$ is defined as the average flux $\langle(\boldsymbol{A}\boldsymbol{\nabla}u_h)\cdot\boldsymbol{n}_e\rangle$.

4.2 Numerical evaluation of the Inf-Sup condition

In order to apply Theorem 2.1 and the estimate (9), we must know the continuity and inf-sup parameters. The continuity condition holds with $M = 1$, i.e.

$$|B(u,v)| \leq \|u\|_V \|v\|_V, \quad (34)$$

where $\|.\|_V$ is the associated norm defined in (22). To verify this, we multiply the integrands appearing on $\Gamma_{\rm int}$ and $\Gamma_{\rm D}$ in the definition of $B(.,.)$ by $h^\alpha h^{-\alpha}$, and use standard inequalities [9] to show that

$$\begin{aligned}
|B(u,v)| \ &\leq\ |u|_1|v|_1 \\
&+\ \left(\left|h^{-\alpha}\,\gamma_0 u\right|^2_{0,\Gamma_{\rm D}} + |h^\alpha\ (\boldsymbol{A}\boldsymbol{\nabla}u)\cdot\boldsymbol{n}|^2_{0,\Gamma_{\rm D}} + \left|h^{-\alpha}\,[\gamma_0 u]\right|^2_{0,\Gamma_{\rm int}} + |h^\alpha\,\langle(\boldsymbol{A}\boldsymbol{\nabla}u)\cdot\boldsymbol{n}\rangle|^2_{0,\Gamma_{\rm int}}\right)^{\frac{1}{2}} \\
&\times\ \left(\left|h^{-\alpha}\,\gamma_0 v\right|^2_{0,\Gamma_{\rm D}} + |h^\alpha\ (\boldsymbol{A}\boldsymbol{\nabla}v)\cdot\boldsymbol{n}|^2_{0,\Gamma_{\rm D}} + \left|h^{-\alpha}\,[\gamma_0 v]\right|^2_{0,\Gamma_{\rm int}} + |h^\alpha\,\langle(\boldsymbol{A}\boldsymbol{\nabla}v)\cdot\boldsymbol{n}\rangle|^2_{0,\Gamma_{\rm int}}\right)^{\frac{1}{2}} \\
&\leq\ \left(|u|_1|v|_1 + |u|_{0,\Gamma_{\mathcal{P}_h}}|v|_{0,\Gamma_{\mathcal{P}_h}}\right),
\end{aligned}$$

Thus, using (22), we obtain

$$|B(u,v)| \leq \|u\|_V \|v\|_V. \quad (35)$$

The behavior of the discrete inf-sup parameter γ_h appearing in (9) as a function of mesh parameters h and p is of paramount importance in determining the stability of the DGM. A straightforward calculation of γ_h for representative cases can be done using the eigenvalue problem described below.

THEOREM 4.1 *Let $\mathcal{H}_h$ be an n-dimensional Hilbert space, and $\boldsymbol{C}_{\mathcal{H}_h} \in \mathbb{R}^n \times \mathbb{R}^n$ the symmetric positive definite matrix associated with the inner product in $\mathcal{H}_h$. Let $B : \mathcal{H}_h \times \mathcal{H}_h \longrightarrow \mathbb{R}$ be a generic bilinear form, and $\boldsymbol{B} \in \mathbb{R}^n \times \mathbb{R}^n$ the associated matrix, then the inf-sup condition associated with $B(.,.)$ can be evaluated using the following eigenvalue problem:*

$$\boxed{\boldsymbol{B}^T \boldsymbol{C}_{\mathcal{H}_h}^{-1} \boldsymbol{B}\, \boldsymbol{u} = \lambda_{\min}\, \boldsymbol{C}_{\mathcal{H}_h} \boldsymbol{u}} \tag{36}$$

from which we obtain the inf-sup constant $\gamma_h = \sqrt{\lambda_{\min}}$. ■

Proof: Given that $\boldsymbol{C}_{\mathcal{H}_h}$ is symmetric and positive definite, it can be factored into lower/upper triangular form $\boldsymbol{C}_{\mathcal{H}_h} = \boldsymbol{U}_{\mathcal{H}_h}^T \boldsymbol{U}_{\mathcal{H}_h}$. Then, the norm in $\mathcal{H}_h$ is related to the Euclidean norm $\|.\|$ in $\mathbb{R}^n$ as follows

$$\|v\|_{\mathcal{H}_h}^2 = \boldsymbol{v}^T \boldsymbol{C}_{\mathcal{H}_h} \boldsymbol{v} = \boldsymbol{v}^T \boldsymbol{U}_{\mathcal{H}_h}^T \boldsymbol{U}_{\mathcal{H}_h} \boldsymbol{v} = \|\boldsymbol{U}_{\mathcal{H}_h} \boldsymbol{v}\|^2, \quad \boldsymbol{v} \in \mathbb{R}^n.$$

Let us now consider the following equalities:

$$\max_{v \in \mathcal{H}_h} \frac{|B(u,v)|}{\|v\|_{\mathcal{H}_h}} = \max_{\boldsymbol{v} \in \mathbb{R}^n} \frac{|(\boldsymbol{v}, \boldsymbol{B}\, \boldsymbol{u})|}{\|\boldsymbol{U}_{\mathcal{H}_h} \boldsymbol{v}\|} = \max_{\boldsymbol{w} \in \mathbb{R}^n} \frac{|(\boldsymbol{w}, \boldsymbol{U}_{\mathcal{H}_h}^{-T} \boldsymbol{B}\, \boldsymbol{u})|}{\|\boldsymbol{w}\|} = \left\| \boldsymbol{U}_{\mathcal{H}_h}^{-T} \boldsymbol{B}\, \boldsymbol{u} \right\|,$$

using this result, we can write the discrete inf-sup constant γ_h as follows:

$$\gamma_h = \min_{u \in \mathcal{H}_h} \max_{v \in \mathcal{H}_h} \frac{|B(u,v)|}{\|u\|_{\mathcal{H}_h} \|v\|_{\mathcal{H}_h}} = \min_{\boldsymbol{u} \in \mathbb{R}^n} \frac{\left\| \boldsymbol{U}_{\mathcal{H}_h}^{-T} \boldsymbol{B}\, \boldsymbol{u} \right\|}{\|\boldsymbol{U}_{\mathcal{H}_h} \boldsymbol{u}\|} = \min_{\boldsymbol{x} \in \mathbb{R}^n} \frac{\left\| \boldsymbol{U}_{\mathcal{H}_h}^{-T} \boldsymbol{B} \boldsymbol{U}_{\mathcal{H}_h}^{-1}\, \boldsymbol{x} \right\|}{\|\boldsymbol{x}\|}, \tag{37}$$

and γ_h can be evaluated by solving the eigenvalue problem (36). ■

4.2.1 One-dimensional study

We consider the simple Dirichlet problem $-u'' = f$ on $(0,1)$, with homogeneous boundary conditions. The following analytical result is proven in [9]:

THEOREM 4.2 *In the space $V_p(\mathcal{P}_h)$, if $p_e \geq 3$, $1 \leq e \leq N(\mathcal{P}_h)$, the bilinear form (25) of the discontinuous Galerkin approximation satisfies*

$$\inf_{u \in V_p} \sup_{v \in V_p} \frac{|B(u,v)|}{\|u\|_V \|v\|_V} \geq \frac{\left(1 - \frac{1}{2}\lambda_o\right)}{\left(1 + \sqrt{\lambda_o + 1}\right)}$$

where $1.23 < \lambda_o < 1.24$ independently of the discretization parameters p_e and h_e.

Remark: Theorem 4.2 was proven for polynomial basis functions of degree ≥ 3. Numerical experiments indicate, however, that the method is stable and convergent for polynomial basis functions of degree ≥ 2.

	Num. of Elements					
p	2	4	8	16	32	64
2	.3333333	.3333333	.3333333	.3333333	.3333333	.3333333
3	.5031162	.5031162	.5031162	.5031162	.5031162	.5031162
4	.5031162	.5031162	.5031162	.5031162	.5031162	.5031162
5	.5039530	.5039530	.5039530	.5039530	.5039530	.5039530
6	.5039530	.5039530	.5039530	.5039530	.5039530	.5039530
7	.5025293	.5025293	.5025293	.5025293	.5025293	.5025293
8	.5025293	.5025293	.5025293	.5025293	.5025293	.5025293

Table 1: Inf-Sup constant for model equation with Dirichlet boundary conditions. Uniform mesh

	Num. of Elements					
p	2	4	8	16	32	64
2	.3333485	.3365059	.3586421	.3460370	.3500695	.3506928
3	.5031302	.5032297	.5034426	.5034566	.5034003	.5033587
4	.5037151	.5032127	.5036960	.5037744	.5035089	.5036255
5	.5039498	.5037831	.5038352	.5037374	.5038389	.5037868
6	.5039400	.5038976	.5038288	.5038620	.5037359	.5037929
7	.5024107	.5024598	.5025075	.5024672	.5023690	.5023519
8	.5025245	.5024703	.5023743	.5024000	.5023425	.5023330

Table 2: Inf-Sup constant for model equation with Dirichlet boundary conditions. Random distribution of mesh points (1/4).

Using (36), we evaluate γ_h for various meshes $\mathcal{P}_h$ and uniform p, $p_e = p$. Results for uniform meshes are collected in Table 1 and for nonuniform meshes in Tables 2 and 3; the data in Table 2 corresponds to an arbitrary distribution of nodes for which the worst aspect ratio between adjacent elements is 1/4, and Table 3 shows the effect of a geometric distribution of mesh points such that $h_{\min}/h_{\max} = 10^{-7}$.

We observe that in all cases, the calculated γ_h is independent of the mesh size, and is independent of p for $p \geq 3$.

The asymptotic values obtained are higher than the analytic value because the latter is only a lower bound of the exact inf-sup constant.

p	Num. of Elements					
	2	4	8	16	32	64
2	.3440400	.3572851	.3650082	.3658733	.3658805	.3658805
3	.5032378	.5033161	.5033382	.5033402	.5033402	.5033402
4	.5034964	.5037628	.5038515	.5038596	.5038596	.5038596
5	.5038662	.5038452	.5038392	.5038387	.5038387	.5038387
6	.5038321	.5037621	.5037426	.5037409	.5037409	.5037409
7	.5024515	.5024277	.5024210	.5024204	.5024204	.5024204
8	.5024281	.5023737	.5023585	.5023572	.5023571	.5023571

Table 3: Inf-Sup constant for model equation with Dirichlet boundary conditions. Geometric distribution of mesh points ($h_{\min}/h_{\max} = 10^{-7}$).

The *a priori* error estimate for this case is given by the following theorem:

THEOREM 4.3 *Let the solution u to (21) $\in H^s(\mathcal{P}_h(\Omega))$, with $s > 3/2$, and $p_{\max} = \max_e(p_e)$. If the approximation properties (19)(20) hold for the spaces $V_p(\mathcal{P}_h)$, then the error of the approximate solution u_{DG} can be bounded as follows:*

$$\|u - u_{DG}\|_V^2 \leq C p_{\max}^2 \sum_{\Omega_e \in \mathcal{P}_h} \left(\frac{h_e^{\mu_e - 1}}{p_e^{s-1}} \|u\|_{s,\Omega_e} \right)^2, \tag{38}$$

where $\mu_e = min(p_e + 1, s)$, and the constant C depends on s and on conditions (11) and (12), but it is independent of u, h_e and p_e.

Proof: See proof of Theorem 4.4 with $\kappa = 0$. ■

4.2.2 Two-dimensional analysis

A two-dimensional study of the behavior of the Inf-Sup parameter γ_h for the discrete case is carried out for meshes with different numbers $N(\mathcal{P}_h)$ of elements, different degrees of skewness, aspect ratios, and for uniform and nonuniform p_e. These experiments are done for a model Dirichlet problems, for Laplace's equation on a parallelogram. Figure 5 shows some of the subdomains on which the value of the Inf-Sup parameter γ_h is computed.

First the Inf-Sup parameter γ_h is evaluated for meshes with uniform p, $p_e = p$, $1 \leq e \leq N(\mathcal{P}_h)$. Tables 4, 5, 6, and 7 show the Inf-Sup parameter γ_h for meshes with aspect ratio 1:1, 1:2, 1:4, and 1:8, respectively. These results indicate that the Inf-Sup parameter γ_h is asymptotically independent of h, but depends on p. Figure 6 shows the Inf-Sup dependence on p for meshes with 64 elements, uniform degree p, aspect ratios 1:1, 1:2, 1:4, 1:8, and

skewness of 90° and 30°. The asymptotic dependence on p (within the range of interest) is $\sim p^{-1}$ for all the meshes with skewness of 90°, and $\sim p^{-1.5}$ for those with skewness of 30°.

Next, the Inf-Sup parameter γ_h is evaluated for meshes with a random distribution of p_e. The distribution starts with $p_e = p_{max}$ for element number 1, for the remaining elements the order is chosen randomly between 2 and p_{max}. Tables 8, 9, 10, and 11 show the Inf-Sup parameter γ_h for meshes with aspect ratio 1:1, 1:2, 1:4, and 1:8, respectively. These results indicate that the Inf-Sup parameter γ_h is not very sensitive to abrupt changes in p. In fact, for orthogonal meshes, the Inf-Sup parameter γ_h is approximately 5 percent larger for most of the meshes where at least one element has $p_e < p_{max}$, i.e. for $p > 2$ and a number of elements ≥ 4. For the skewed meshes, for a few cases the Inf-Sup parameter γ_h is less than 1 percent smaller than the corresponding value when $p_e = p_{max}$ for all the elements, and in many cases it is larger. Figure 6 shows the Inf-Sup dependence on p for meshes with 64 elements, random distribution of p_e, aspect ratios 1:1, 1:2, 1:4, 1:8, and skewness of 90° and 30°. The asymptotic dependence on p (within the range of interest) is again $\sim p^{-1}$ for all the meshes with skewness of 90°, and $\sim p^{-1.5}$ for those with skewness of 30°.

From the above studies, it is clear that the Inf-Sup parameter γ_h is asymptotically independent of h but depends on p. The dependence on p is not considered to be significant for practical calculations, since the loss of $O(p)$ accuracy can be offset by the better approximation achieved ($O(h^p)$) using high p for cases with high regularity. By assuming that $\gamma_h = \mathrm{O}\left(p_{\max}^{-\kappa}\right)$, $\kappa \geq 0$, an estimate of the global rates of convergence of the DGM can be easily estimated. We have:

THEOREM 4.4 *Let the solution u to (21) $\in H^s\left(\mathcal{P}_h\left(\Omega\right)\right)$, with $s > 3/2$, and assume that the value of the inf-sup parameter is $\gamma_h = C_p\, p_{\max}^{-\kappa}$ with $\kappa \geq 0$ and $p_{\max} = \max_e(p_e)$. If the approximation properties (19)(20) hold for the spaces $V_p\left(\mathcal{P}_h\right)$, then the error of the approximate solution u_{DG} can be bounded as follows:*

$$\left\|u - u_{DG}\right\|_V^2 \leq C p_{\max}^{2(\kappa+1)} \sum_{\Omega_e \in \mathcal{P}_h} \left(\frac{h_e^{\mu_e - 1}}{p_e^{s-1}} \left\|u\right\|_{s,\Omega_e} \right)^2, \tag{39}$$

where $\mu_e = min(p_e + 1, s)$, and the constant C depends on s and on conditions (11) and (12), but it is independent of u, h_e and p_e.

Proof: Given that $u \in P_{p_e}\left(\Omega_e\right)$, we can use the estimate introduced in (20) for norms defined on the boundaries, and we bound $\left\|u\right\|_V$ as follows

$$\left\|u\right\|_V^2 \leq \left|u\right|_{1,\mathcal{P}_h}^2 + C_0 \sum_{\Omega_e \in \mathcal{P}_h} p_e^2 \left\| h_e^{-1} u \right\|_{0,\Omega_e}^2 + C_1\, p_{\max}^2 \left|u\right|_{1,\mathcal{P}_h}^2$$

$$\leq \max(C_0, 1 + C_1)\, p_{\max}^2 \left(\left|u\right|_{1,\mathcal{P}_h}^2 + \sum_{\Omega_e \in \mathcal{P}_h} \left\| h_e^{-1} u \right\|_{0,\Omega_e}^2 \right),$$

$$|u|^2_{1,\mathcal{P}_h} \leq \|u\|^2_V \leq C p^2_{\max} \left(\sum_{\Omega_e \in \mathcal{P}_h} \left\| h_e^{-1} u \right\|^2_{0,\Omega_e} + |u|^2_{1,\mathcal{P}_h} \right). \tag{40}$$

Using the approximation estimate presented in (19) and bound (40), there exists a local polynomial approximation u_p of $u \in H^s(\mathcal{P}_h(\Omega))$ in the norm $\|.\|_V$ such that:

$$\|u - u_p\|^2_V \leq C p^2_{\max} \sum_{\Omega_e \in \mathcal{P}_h} \left(\frac{h_e^{\mu_e - 1}}{p_e^{s-1}} \|u\|_{s,\Omega_e} \right)^2, \quad s > 3/2, \quad \mu_e = min(p_e + 1, s).$$

Finally, using the continuity and inf-sup parameters, and assuming that the exact solution $u \in H^s(\mathcal{P}_h)$, we arrive at the following *a priori* error estimate:

$$\|u - u_{DG}\|^2_V \leq \left(1 + \frac{M}{\gamma_h}\right)^2 \inf_{w_p \in V_p} \|u - w_p\|^2_V \leq C\, p^{2(\kappa+1)}_{\max} \sum_{\Omega_e \in \mathcal{P}_h} \left(\frac{h_e^{\mu_e - 1}}{p_e^{s-1}} \|u\|_{s,\Omega_e} \right)^2,$$

where $s > 3/2$, $\mu_e = min(p_e + 1, s)$, and C depends on s but is independent of u, h_e, and p_e. ■

Remark 4.1 *The error estimate (39) is a bound for the worst possible case, including all possible data. For a wide range of data, however, the error estimate (39) may be pessimistic, and the actual rate of convergence can be larger than that suggested by the above bound.*

The value of the parameter κ depends on the dimension d. For $d = 1$, $\kappa = 0$ [9], whereas for $d = 2$ the value depends on the mesh regularity; numerical evidence suggests that for the cases considered, the value $\kappa \approx 1.0 - 1.5$. ■

5 Numerical experiments

We shall now examine experimentally the performance of the DGM for several representative examples.

5.1 Two-Point BV problems:

We will first analyze test cases of the following type:

$$\begin{cases} -\dfrac{\mathrm{d}^2 u}{\mathrm{d}x^2} = S & \text{on } [0,1] \\ \\ u(x) = 0 & \text{at } x = 0 \text{ and } x = 1 \end{cases} \tag{41}$$

First we consider problem (41) with $S = (4\pi)^2 \sin(4\pi x)$, for which the exact solution is $u_{exact}(x) = \sin(4\pi x)$. Figure 7 shows error in the norm $\|.\|_V$ and h convergence rate for uniform meshes. Figure 8 shows error and h convergence rate for nonuniform meshes obtained by successive refinements of an initial grid with a subsequent random displacement of value $\pm 0.20h$ to each interior node. These figures show an asymptotic convergence rate of order $\mathrm{O}(h^p)$ in agreement with Theorem 4.3. Note: the h convergence rate is given by

$$CR_h = \frac{\log(e_{2h}/e_h)}{\log(2)}, \quad e_h = \|u_h - u_{ex}\|_V.$$

The next test cases measure the error in the L^2-norm. Problem (41) is solved with $S = (2\pi)^2 \sin(2\pi x)$ on uniform meshes, Fig. 9 shows error in the L^2-norm and h convergence rate. These figures indicate an asymptotic convergence rate of order $\mathrm{O}(h^{p+1})$ for p odd and $\mathrm{O}(h^p)$ for p even. This test did not involve $p > 7$ because after the first mesh refinement the error was $\| e \| < 10^{-13}$. Next, problem (41) is solved on a nonuniform grid ($\pm 0.20h$) with $S = (6\pi)^2 \sin(6\pi x)$. Figure 10 shows error and h convergence rate, it is clear from these figures that the asymptotic convergence rate do not deteriorate for nonuniform grids. The numerical convergence rates agree with the upper bound of order $\mathrm{O}(h^p)$ obtained in [8].

The following test case deals with h and p convergence rates in the H^1 seminorm. This test case is the solution to problem (41) with $S = (3\pi)^2 \sin(3\pi x)$, for which the exact solution is $u_{exact}(x) = 1 + \sin(3\pi x)$.

We define the $p-$convergence rate (CR_p) as

$$CR_p = \frac{\log(e_p/e_{p+1})}{\log(1 + 1/p)}, \quad e_p = |u - u_{ex}|_1, \quad p \geq 2,$$

Figure 11 shows h and p convergence rates in the H^1 seminorm. From these figures, it is evident that the h convergence rate is *optimal*, i.e. $\mathrm{O}(h^p)$. The behavior of the p-convergence rate can be estimated by considering that the error in $|.|_1$ is $e_p \approx h^p/(p!)$, then $CR_p \approx p \log((p+1)/h)$, which is the asymptotic convergence rate shown in the figure.

5.2 2-D Experiments:

The first test case is the solution to the following Poisson problem:

$$\begin{cases} -\Delta u = 4(1 - x^2 - y^2)\ \exp(-(x^2 + y^2)) & \text{in } \Omega \\ \\ u(x, y) = \exp(-(x^2 + y^2)) & \text{on } \partial\Omega \end{cases}$$

where Ω is the subdomain shown in Fig. 3. The h convergence rate is evaluated by successive global refinements of the domain.

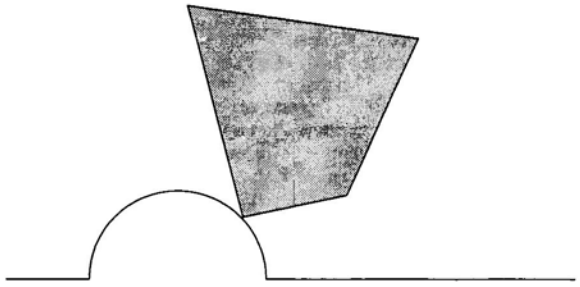

Figure 3: Subdomain for successive global refinements.

Figure 12 shows the L^2-norm of the error and the convergence rate. It is clear from these figures that a convergence rate of order $\mathrm{O}\left(h^{p+1}\right)$ is obtained for p odd. For p even, however, results indicate that for low p the h convergence rate tends to $\mathrm{O}\left(h^{p}\right)$, but for high p it tends to $\mathrm{O}\left(h^{p+1}\right)$.

The second test case involves h-p adaptation for a case with low regularity, which is a Dirichlet problem defined on the L-shaped domain shown in Fig. 4, with boundary values given by $u = r^{2/3}\ \sin(2\theta/3)$, which is a solution to Laplace's equation.

The p adaptation process was implemented as follows: for every element Ω_e that is refined, we keep track of the maximum values of $[(\boldsymbol{A}\boldsymbol{\nabla}u)\cdot\boldsymbol{n}]$ and $[u]$ on $\partial\Omega_e$. If the characteristic size of the element h_{new} in the current adaptation cycle is smaller than the previous value h_{old} (inherited from the parent element), and if the following equations hold

$$\frac{\log\left([(\boldsymbol{A}\boldsymbol{\nabla}u)\cdot\boldsymbol{n}]^{old}_{max}/[(\boldsymbol{A}\boldsymbol{\nabla}u)\cdot\boldsymbol{n}]^{new}_{max}\right)}{\log\left(h_{old}/h_{new}\right)} < C\ \min_{e=1}^{Neig}(p_e),$$

$$\frac{\log\left([u]^{old}_{max}/[u]^{new}_{max}\right)}{\log\left(h_{old}/h_{new}\right)} < C\ \left(\min_{e=1}^{Neig}(p_e)+1\right),$$

where C is a tolerance of value 0.85, then the order p is reduced.

The error indicator for h refinement is as follows: for every element Ω_e in the mesh, the integral on $\partial\Omega_e$ of $|[(\boldsymbol{A}\boldsymbol{\nabla}u)\cdot\boldsymbol{n}]|$ and $|[u]|$ is computed. Then the max and min values of these indicators over the partition $\mathcal{P}_h(\Omega)$ are computed. If the value of any indicator associated

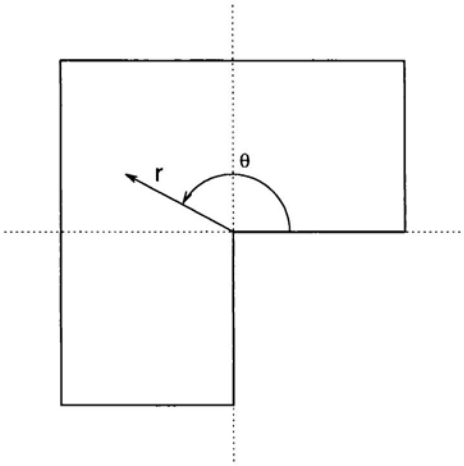

Figure 4: L-shaped domain - Nomenclature.

with a given element is within a given (specified) percentage of the max value, then the element is refined.

In the following test, the h-p adaptive process is initiated with a mesh consisting of three square elements of size 1×1 and monomial basis of order 5. The purpose of this test is to check if the code detects a low h-convergence rate and decreases the monomial order accordingly. Figure 13 (top) shows the resulting p distribution and h refinement, and (bottom) a 20-times magnification at the corner showing pointwise error. It is clear that the low regularity of the solution is detected because the order p is minimum (i.e. $p = 2$ for stability reasons) for most of the elements.

As another test, we attempt to evaluate the sensitivity (loss of stability) of the method to $p-$enrichment in zones with low regularity. In this case, the p distribution is obtained by forcing $p-$enrichment where low regularity is detected (opposed to the usual procedure). Figure 14 shows with a magnification of 20-times the p distribution (top), and the corresponding pointwise error (bottom). From this experiment, it is clear that the method can accommodate $p-$enrichments even in zones with low regularity without stability problems.

Finally, we compare the convergence rates using uniform and adaptive refinements. Figure 17 shows the convergence rate using uniform p with global uniform refinements, and using adaptive h- and p-adaptation. The convergence rate of the uniform h refinement is exactly equal to the theoretical value $N^{-1/3}$ in the H^1 seminorm, and the convergence rates of the h-adaptation is close to the theoretical maximum which is N^{-1} in the H^1 seminorm. The exponential convergence rates shown (as h-p *sqrt*) are obtained by setting the polynomial order as $p_e = [2 + 7(r_e^2/2)^{0.3}]$, where r_e represents the radius of the element's baricenter, and

[.] is the integer part.

In summary, the numerical experiments confirm the robustness of the method under many different conditions. For the class of problems considered, the method appears to be stable even for arbitrary distributions of spectral orders and very different element sizes and aspect ratios.

6 Concluding comments

As a brief summary of the major observations of this study, we list the following:

- diffusion dominated problems can be solved using piecewise discontinuous basis functions, without using auxiliary variables such as fluxes in mixed methods. The discontinuous Galerkin method developed herein involves imposing weak continuity requirements on interelement boundaries; both solution values and fluxes are discontinuous across these interfaces;
- The method resembles hybrid and interior penalty methods, but no Lagrange multiplier or penalty parameter appears in the formulation;
- The method appears to be robust, exhibiting only a small loss of accuracy in H^1 in which stretching and distortion of elements results in a suboptimal rate of $p-$convergence; numerical experiments suggest that the inf-sup parameter $\gamma_h \approx \mathrm{O}\left(p^{-1}\right)$ for 2-D cases and γ_h is constant for 1-D problems;
- The behavior of the method in L^2 is different for odd or even order polynomial approximations; for regular mesh refinements in 2-D, the L^2-rate of convergence is experimentally found to be $\mathrm{O}\left(h^{p+1}\right)$ for p odd and $\mathrm{O}\left(h^{p}\right)$ for p even, $p \geq 2$.
- the conditions under which the method is stable and convergent are studied herein, with corresponding *a priori* error estimates, and tests confirm that the method can exhibit high rates of $h-$, $p-$, and $hp-$version convergence.
- coupled with the classical discontinuous Galerkin formulation for transport dominated problems, this formulation is applicable to a wide range of problems, from convection dominated to diffusion dominated cases [9];
- the formulation renders a numerical approximation which is elementwise conservative, and, as such, is, to the best of our knowledge, the first high-order finite element method ever developed with this property;
- the associated bilinear form renders a positive definite and well-conditioned matrix, thus allowing the use of standard iterative methods for high p and for distorted elements;

- this formulation should be particularly convenient for time-dependent problems, because the global mass matrix is *block diagonal,* with *uncoupled* blocks (see [9]).

Acknowledgement

The support of this work by the Army Research Office under grant DAAH04-96-0062 is greatfully acknowledged.

References

[1] D. N. Arnold. An interior penalty finite element method with discontinuous elements. *SIAM J. Numer. Anal.*, 19(4):742–760, August 1982.

[2] A.K. Aziz and I. Babuška. *The Mathematical Foundations of the Finite Element Method with Applications to Partial Differential Equations.* Academic Press, 1972.

[3] I. Babuska and M. Suri. The hp-version of the finite element method with quasiuniform meshes. *Mathematical Modeling and Numerical Analysis*, 21:199–238, 1987.

[4] I. Babuška. The finite element method with lagrangian multipliers. *Numer. Math.*, (20):179–192, 1973.

[5] I. Babuška. Estimates for norms on finite element boundaries. TICAM Forum Notes 6, August 1997.

[6] I. Babuška, J. T. Oden, and J. K. Lee. Mixed-hybrid finite element approximations of second-order elliptic boundary-value problems. *Methods in Applied Mechanics and Engineering*, 11:176–206, 1977.

[7] I. Babuška, J. T. Oden, and J. K. Lee. Mixed-hybrid finite element approximations of second-order elliptic boundary-value problems, part 2 - weak-hybrid methods. *Computer Methods in Applied Mechanics and Engineering*, 14:1–22, 1978.

[8] I. Babuška, J. Tinsley Oden, and C. E. Baumann. A discontinuous *hp* finite element method for diffusion problems: 1-d analysis. TICAM Report 97-22, 1997.

[9] C.E. Baumann. *An hp-Adaptive Discontinuous Finite Element Method for Computational Fluid Dynamics.* PhD dissertation, The University of Texas at Austin, Aug 1997.

[10] L.M. Delves and C.A. Hall. An implicit matching principle for global element calculations. *J. Inst. Math. Appl.*, 23:223–234, 1979.

[11] J.A. Hendry and L.M. Delves. The global element method applied to a harmonic mixed boundary value problem. *J. Comp. Phys.*, 33:33–44, 1979.

[12] J. Nitsche. Über ein Variationsprinzip zur Lösung von Dirichlet Problemen bei Verwendung von Teilräumen, die keinen Randbedingungen unterworfen sind. *Abh. Math. Sem. Univ. Hamburg*, 36:9–15, 1971.

[13] J. T. Oden and G. F. Carey. *Texas Finite Elements Series Vol. IV - Mathematical Aspects*. Prentice-Hall, 1983.

[14] P. Percell and M.F. Wheeler. A local residual finite element procedure for elliptic equations. *SIAM J. Numer. Anal.*, 15(4):705–714, August 1978.

[15] M.F. Wheeler. An elliptic collocation-finite element method with interior penalties. *SIAM J. Numer. Anal.*, 15(4):152–161, 1978.

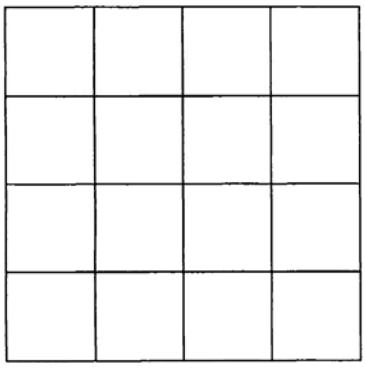

Angle 90, aspect ratio 1:1

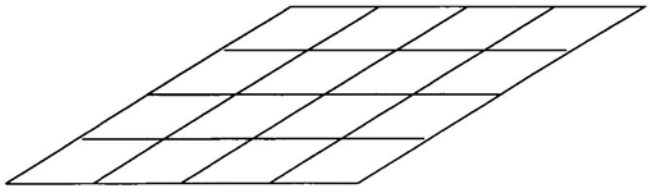

Angle 30, aspect ratio 1:1

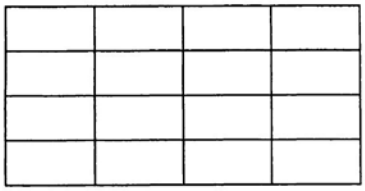

Angle 90, aspect ratio 1:2

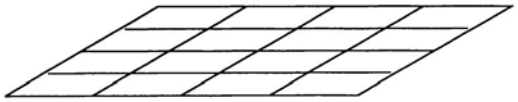

Angle 30, aspect ratio 1:2

Angle 90, aspect ratio 1:4

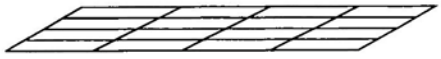

Angle 30, aspect ratio 1:4

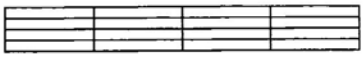

Angle 90, aspect ratio 1:8

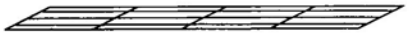

Angle 30, aspect ratio 1:8

Figure 5: Two dimensional stability analysis: domains.

	Angle 90°				**Angle** 30°			
	Num. of Elements				Num. of Elements			
p	1	4	16	64	1	4	16	64
2	.22727	.22728	.22727	.22728	.11493	.12867	.14003	.14091
3	.21262	.21262	.21262	.21262	.07490	.09041	.09159	.09159
4	.14516	.14515	.14515	.14517	.05169	.06047	.06184	.06187
5	.14107	.14107	.14071	.14069	.03826	.04372	.04419	.04418
6	.10226	.10228	.10227	.10230	.02921	.03278	.03307	.03308
7	.09369	.09369	.09369	.09371	.02269	.02532	.02548	.02545
8	.07356	.07358	.07357	.07360	.01819	.01999	.02014	.02011
9	.06438	.06435	.06438	.06440	.01477	.01622	.01634	.01636

Table 4: Inf-Sup constant for Laplace's equation with Dirichlet boundary conditions. Aspect ratio 1:1

	Angle 90°				**Angle** 30°			
	Num. of Elements				Num. of Elements			
p	1	4	16	64	1	4	16	64
2	.24000	.24000	.23999	.24001	.11313	.13062	.13710	.13711
3	.17251	.17252	.17252	.17251	.07296	.08580	.08956	.08959
4	.16103	.16105	.16105	.16104	.05168	.05999	.06055	.06057
5	.11504	.11503	.11503	.11505	.03806	.04334	.04384	.04383
6	.09975	.09975	.09976	.09974	.02896	.03252	.03282	.03290
7	.08552	.08551	.08550	.08548	.02274	.02523	.02547	.02544
8	.06942	.06943	.06942	.06945	.01822	.01996	.02013	.02017
9	.06058	.06056	.06061	.06065	.01485	.01617	.01632	.01630

Table 5: Inf-Sup constant for Laplace's equation with Dirichlet boundary conditions. Aspect ratio 1:2

	Angle 90°				Angle 30°			
	Num. of Elements				Num. of Elements			
p	1	4	16	64	1	4	16	64
2	.15189	.15190	.15189	.15191	.08135	.09446	.09947	.10065
3	.17887	.17889	.17888	.17888	.06720	.07981	.07996	.08012
4	.12623	.12622	.12622	.12623	.04934	.05680	.05777	.05781
5	.10724	.10721	.10722	.10720	.03712	.04155	.04191	.04189
6	.08719	.08719	.08715	.08715	.02875	.03174	.03189	.03185
7	.06953	.06956	.06955	.06957	.02273	.02487	.02512	.02510
8	.06002	.06005	.06005	.06009	.01824	.01992	.01992	.01996
9	.05347	.05345	.05347	.05349	.01495	.01628	.01621	.01625

Table 6: Inf-Sup constant for Laplace's equation with Dirichlet boundary conditions. Aspect ratio 1:4

	Angle 90°				Angle 30°			
	Num. of Elements				Num. of Elements			
p	1	4	16	64	1	4	16	64
2	.08479	.08482	.08482	.08479	.04412	.05613	.05695	.05751
3	.10876	.10879	.10877	.10876	.04925	.05284	.05232	.05287
4	.10319	.10320	.10321	.10319	.04164	.04702	.04648	.04680
5	.09273	.09272	.09271	.09274	.03373	.03861	.03838	.03838
6	.07318	.07315	.07314	.07316	.02706	.02982	.02998	.03009
7	.06187	.06187	.06189	.06172	.02177	.02333	.02336	.02332
8	.05179	.05183	.05177	.05179	.01788	.01898	.01896	.01892
9	.04275	.04280	.04279	.04283	.01498	.01582	.01598	.01560

Table 7: Inf-Sup constant for Laplace's equation with Dirichlet boundary conditions. Aspect ratio 1:8

	Angle 90°				**Angle 30°**			
	Num. of Elements				Num. of Elements			
p	1	4	16	64	1	4	16	64
2	.22727	.22728	.22727	.22728	.11493	.12867	.14003	.14091
3	.21262	.22728	.22727	.22727	.07490	.09374	.09291	.09341
4	.14516	.18369	.18183	.18122	.05169	.06177	.06128	.06125
5	.14107	.15742	.15676	.15520	.03826	.04378	.04379	.04383
6	.10226	.12250	.12243	.11633	.02921	.03284	.03280	.03315
7	.09369	.10164	.10165	.10185	.02269	.02543	.02540	.02532
8	.07356	.08295	.08294	.08202	.01819	.02018	.02010	.02015
9	.06438	.06894	.06852	.06874	.01477	.01620	.01631	.01627

Table 8: Inf-Sup constant for Laplace's equation with Dirichlet boundary conditions. Random distribution of p. Aspect ratio 1:1

	Angle 90°				**Angle 30°**			
	Num. of Elements				Num. of Elements			
p	1	4	16	64	1	4	16	64
2	.24000	.24000	.23999	.24001	.11313	.13062	.13710	.13711
3	.17251	.21106	.20320	.21699	.07296	.08909	.08946	.08941
4	.16103	.18634	.18626	.18617	.05168	.06033	.06021	.06023
5	.11504	.14124	.14122	.13927	.03806	.04373	.04370	.04376
6	.09975	.11811	.11788	.11743	.02896	.03265	.03255	.03292
7	.08552	.09589	.09604	.09612	.02274	.02519	.02533	.02539
8	.06942	.07840	.07857	.07859	.01822	.01999	.02015	.02014
9	.06058	.06541	.06500	.06533	.01485	.01618	.01621	.01626

Table 9: Inf-Sup constant for Laplace's equation with Dirichlet boundary conditions. Random distribution of p. Aspect ratio 1:2

	Angle 90°				**Angle** 30°			
	Num. of Elements				Num. of Elements			
p	1	4	16	64	1	4	16	64
2	.15189	.15190	.15189	.15191	.08135	.09446	.09947	.10065
3	.17887	.18781	.18809	.18833	.06720	.08577	.08328	.08721
4	.12623	.15375	.15415	.15416	.04934	.05751	.05666	.05672
5	.10724	.12621	.12705	.12700	.03712	.04181	.04183	.04209
6	.08719	.10039	.10119	.09453	.02875	.03225	.03205	.03210
7	.06953	.08221	.08258	.08265	.02273	.02502	.02501	.02490
8	.06002	.06831	.06872	.06879	.01824	.01995	.02004	.02001
9	.05347	.05772	.05720	.05723	.01495	.01635	.01616	.01612

Table 10: Inf-Sup constant for Laplace's equation with Dirichlet boundary conditions. Random distribution of p. Aspect ratio 1:4

	Angle 90°				**Angle** 30°			
	Num. of Elements				Num. of Elements			
p	1	4	16	64	1	4	16	64
2	.08479	.08482	.08482	.08479	.04412	.05613	.05695	.05751
3	.10876	.10915	.10922	.10923	.04925	.05531	.05601	.05519
4	.10319	.10552	.09835	.09644	.04164	.05043	.05081	.05175
5	.09273	.10518	.10591	.10610	.03373	.03907	.03854	.03914
6	.07318	.08122	.07689	.07659	.02706	.03024	.03002	.03036
7	.06187	.06776	.06860	.06865	.02177	.02386	.02397	.02389
8	.05179	.05588	.05752	.05749	.01788	.01954	.01966	.01962
9	.04275	.04787	.04759	.04751	.01498	.01606	.01612	.01609

Table 11: Inf-Sup constant for Laplace's equation with Dirichlet boundary conditions. Random distribution of p. Aspect ratio 1:8

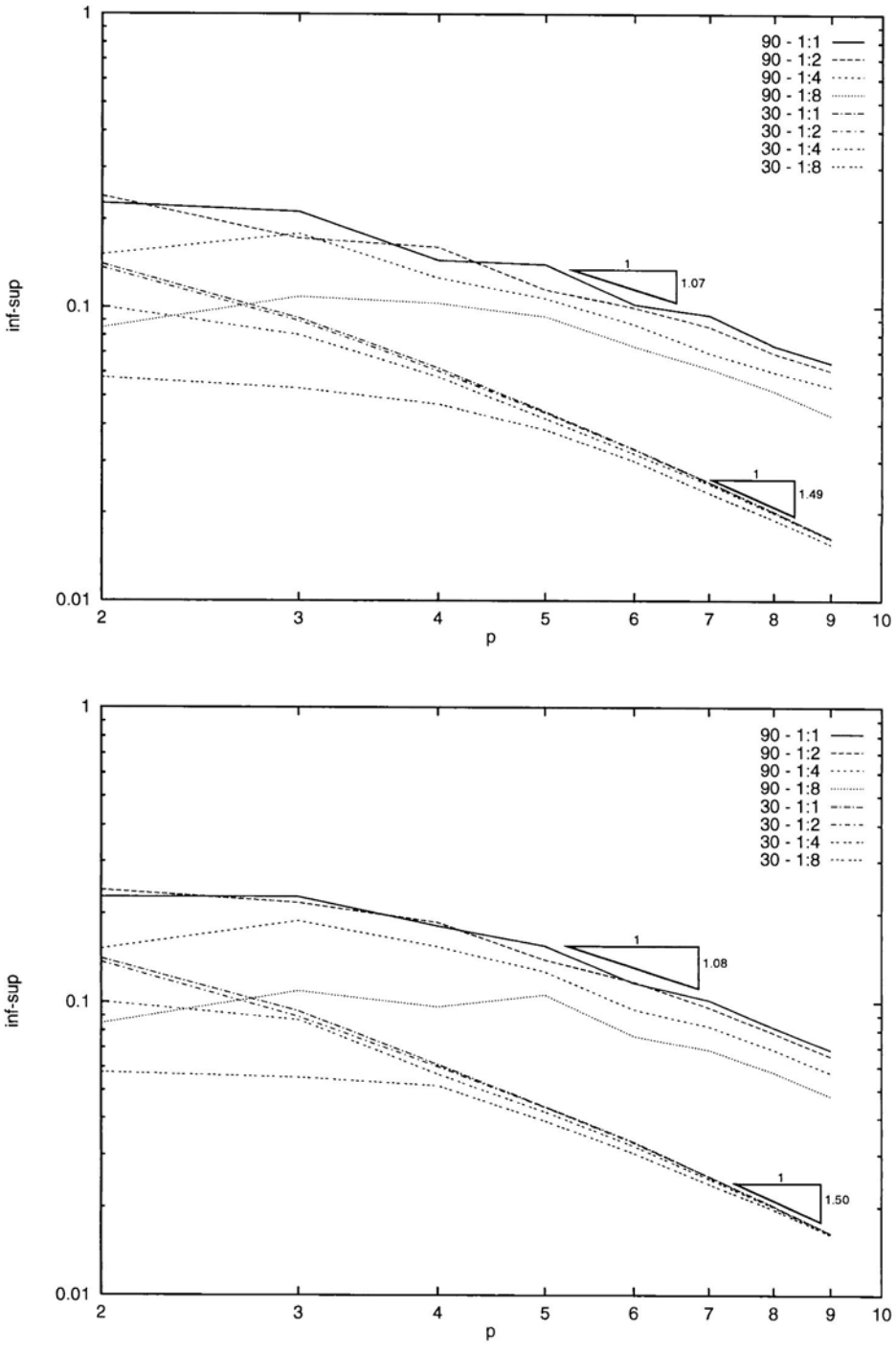

Figure 6: Inf-Sup values for a mesh with 64 elements. Top: uniform p, Bottom: random distribution of p.

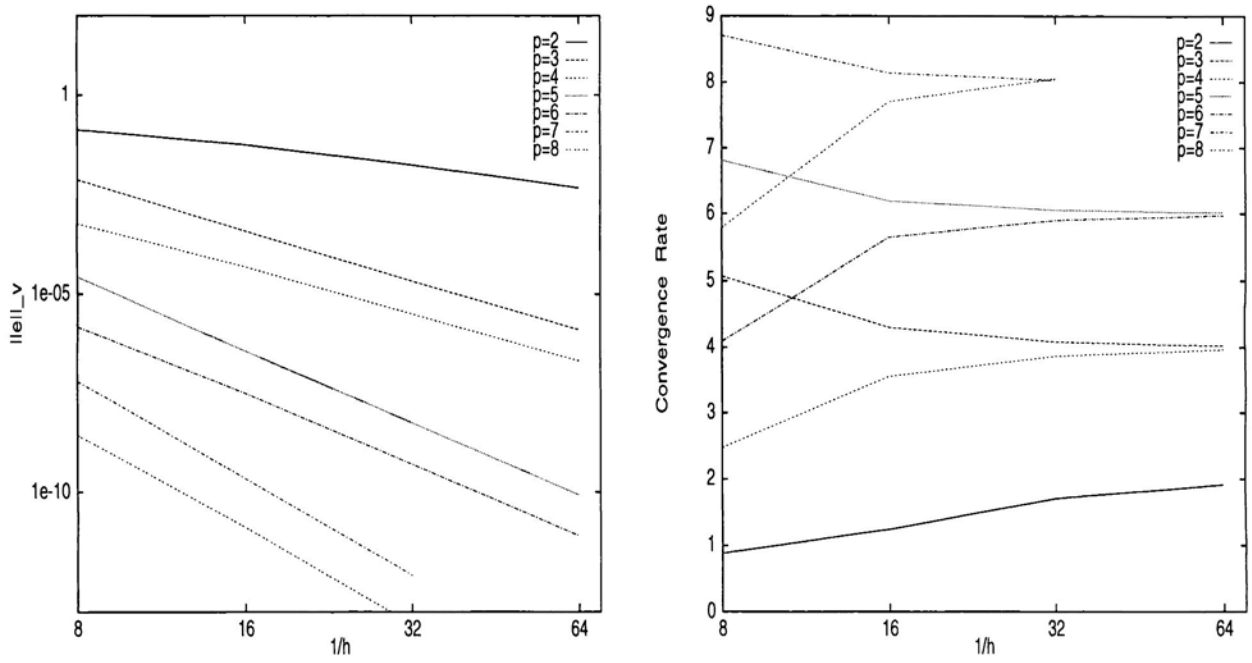

Figure 7: V-norm of the error and convergence rate with uniform meshes:
$-\partial^2 u/\partial x^2 = S$, $S = (4\pi)^2 \sin(4\pi x)$

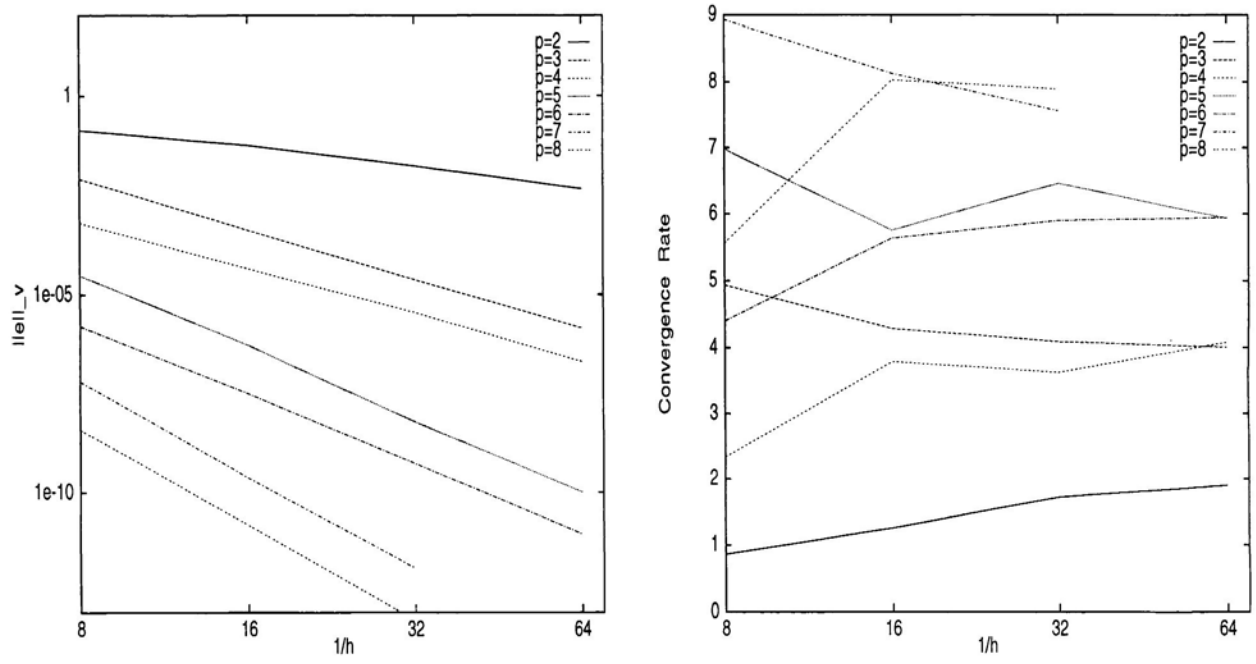

Figure 8: V-norm of the error and convergence rate with nonuniform meshes:
$-\partial^2 u/\partial x^2 = S$, $S = (4\pi)^2 \sin(4\pi x)$, $\delta h = \pm 20\%$.

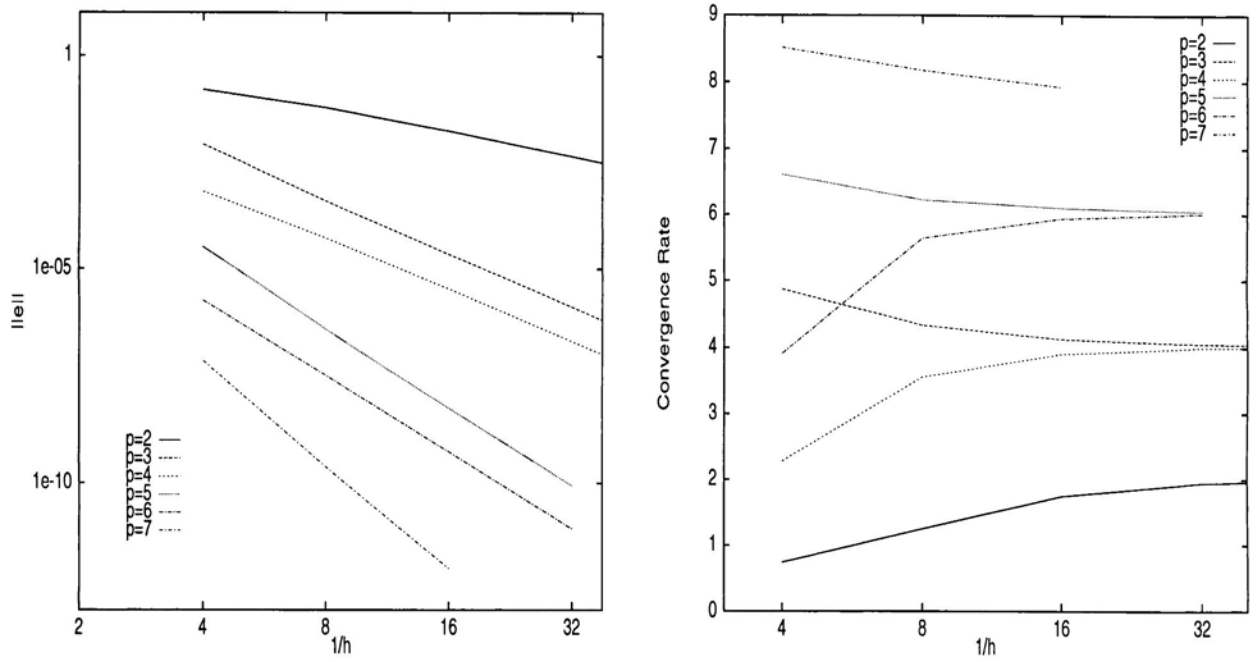

Figure 9: L^2-norm of the error and convergence rate with uniform meshes:
$-\partial^2 u/\partial x^2 = S$, $S = (2\pi)^2 \sin(2\pi x)$

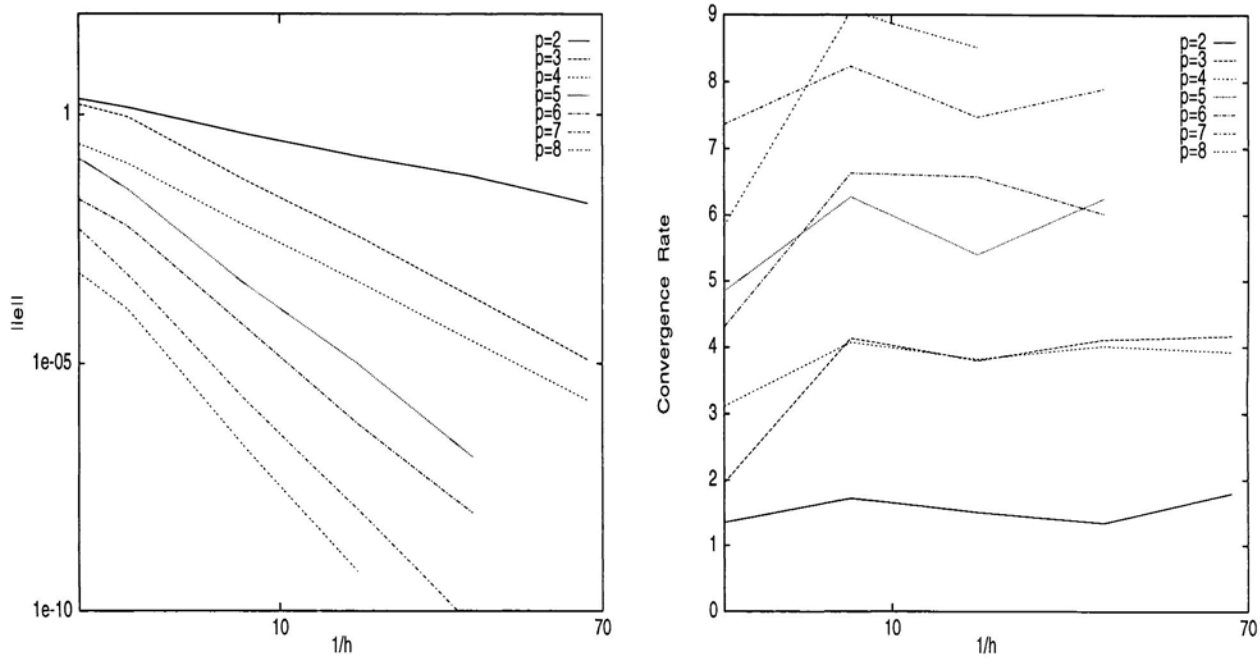

Figure 10: L^2-norm of the error and convergence rate with nonuniform meshes:
$-\partial^2 u/\partial x^2 = S$, $S = (6\pi)^2 \sin(6\pi x)$, $\delta h = \pm 20\%$.

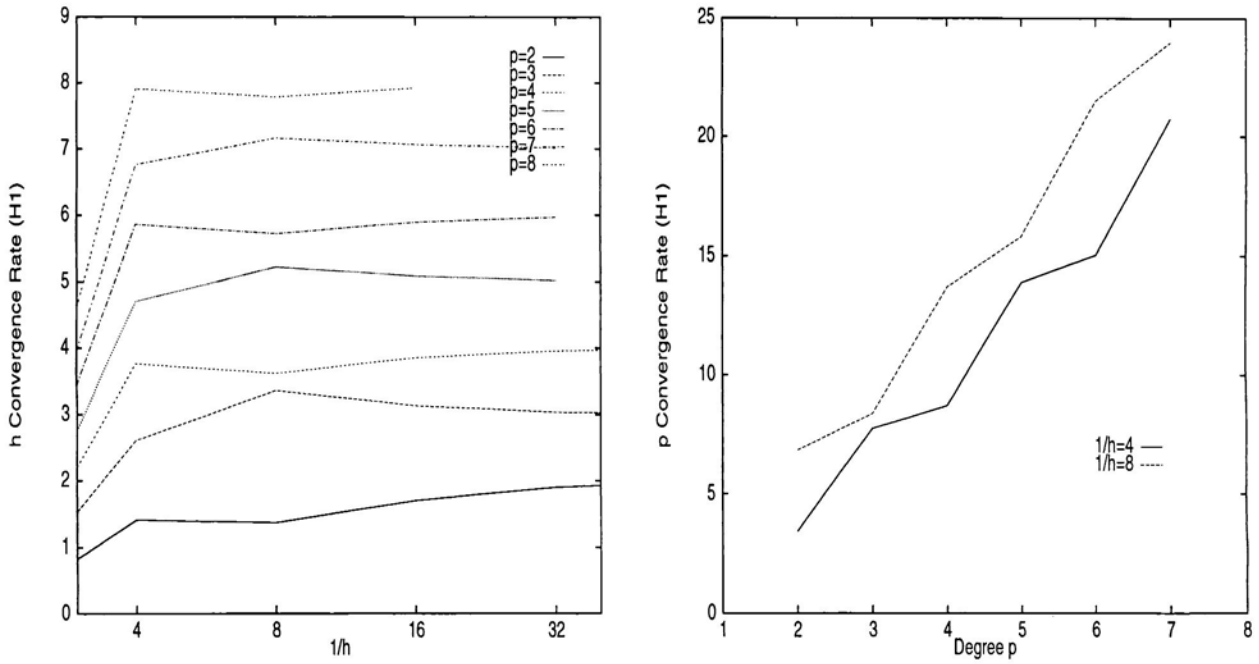

Figure 11: h and p convergence rates in the H^1 seminorm :
$-\partial^2 u/\partial x^2 = S, \quad S = (3\pi)^2 \sin(3\pi x)$

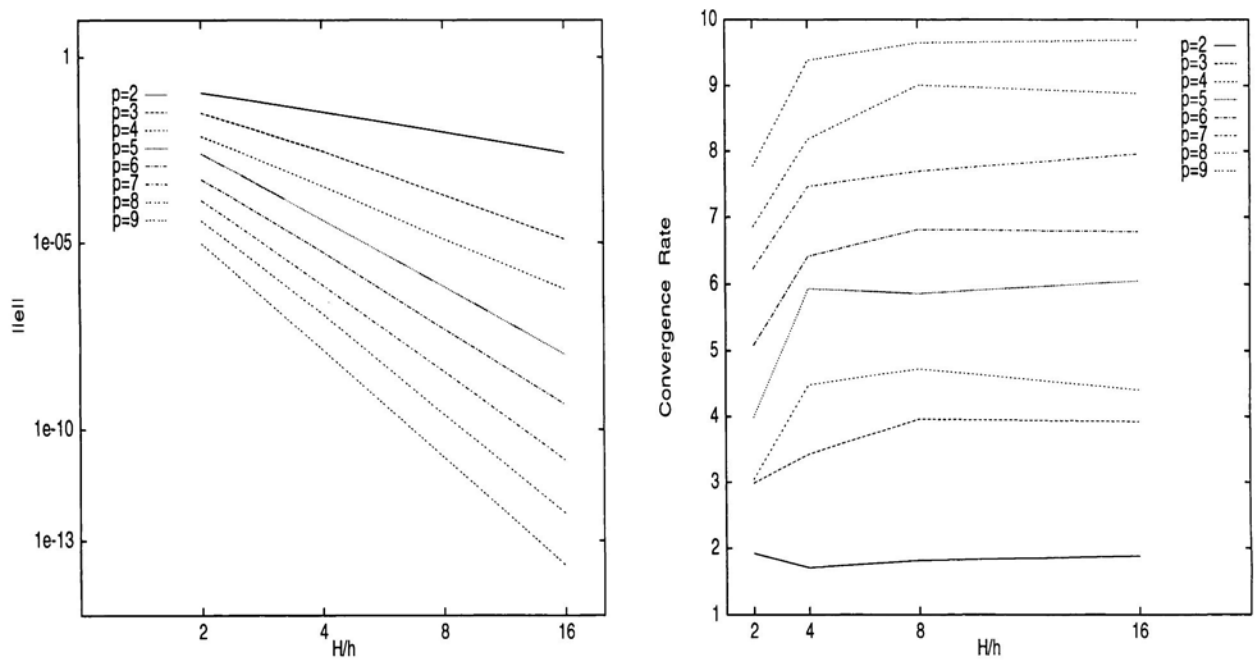

Figure 12: Distorted domain: $-\Delta\psi = S, \quad S = -\Delta(\exp(-(x^2+y^2)))$

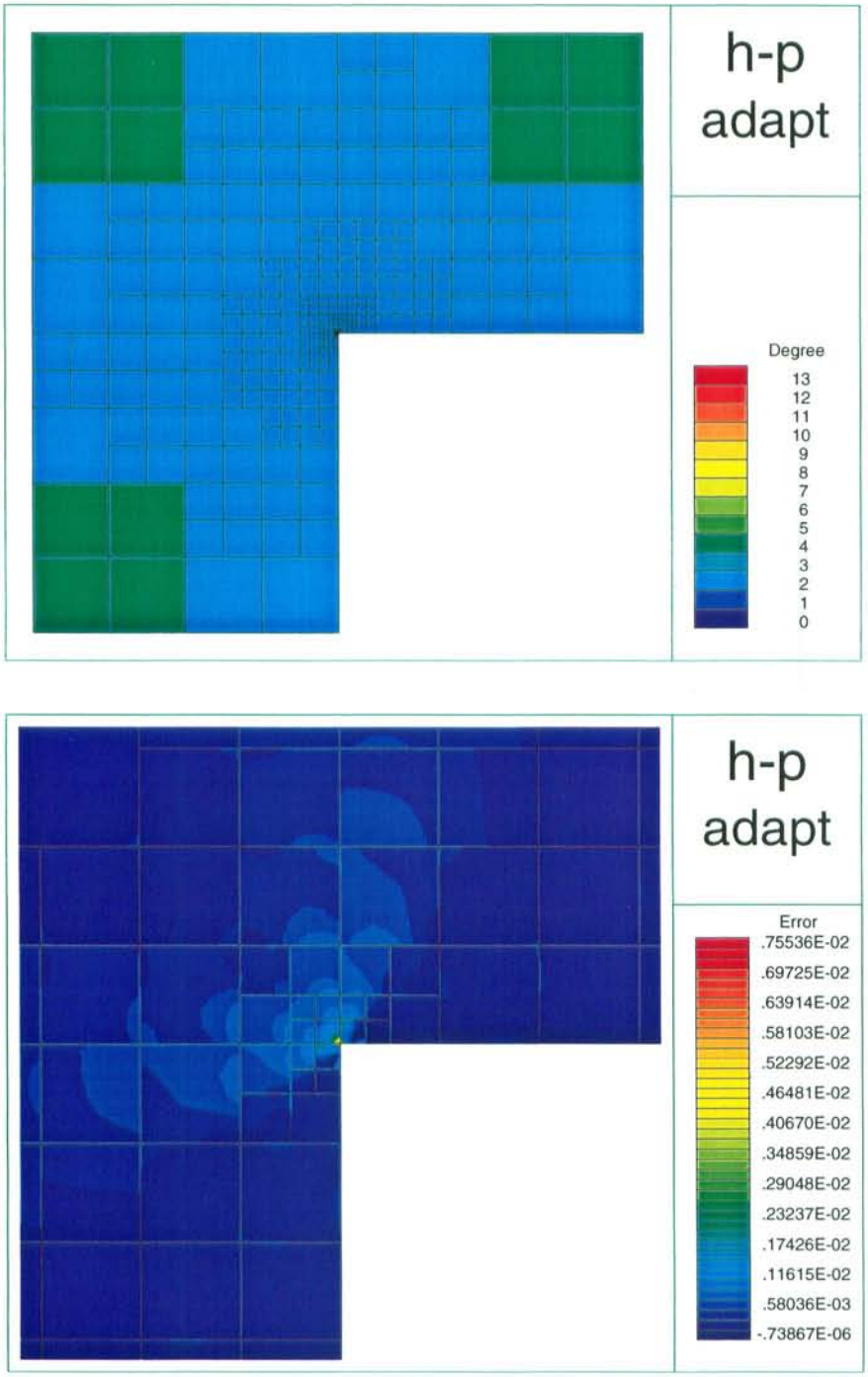

Figure 13: L-Shape domain: Top: Mesh and monomial basis after h-p adaptation, Bottom: ($\times 20$ at the corner) Pointwise error and mesh.

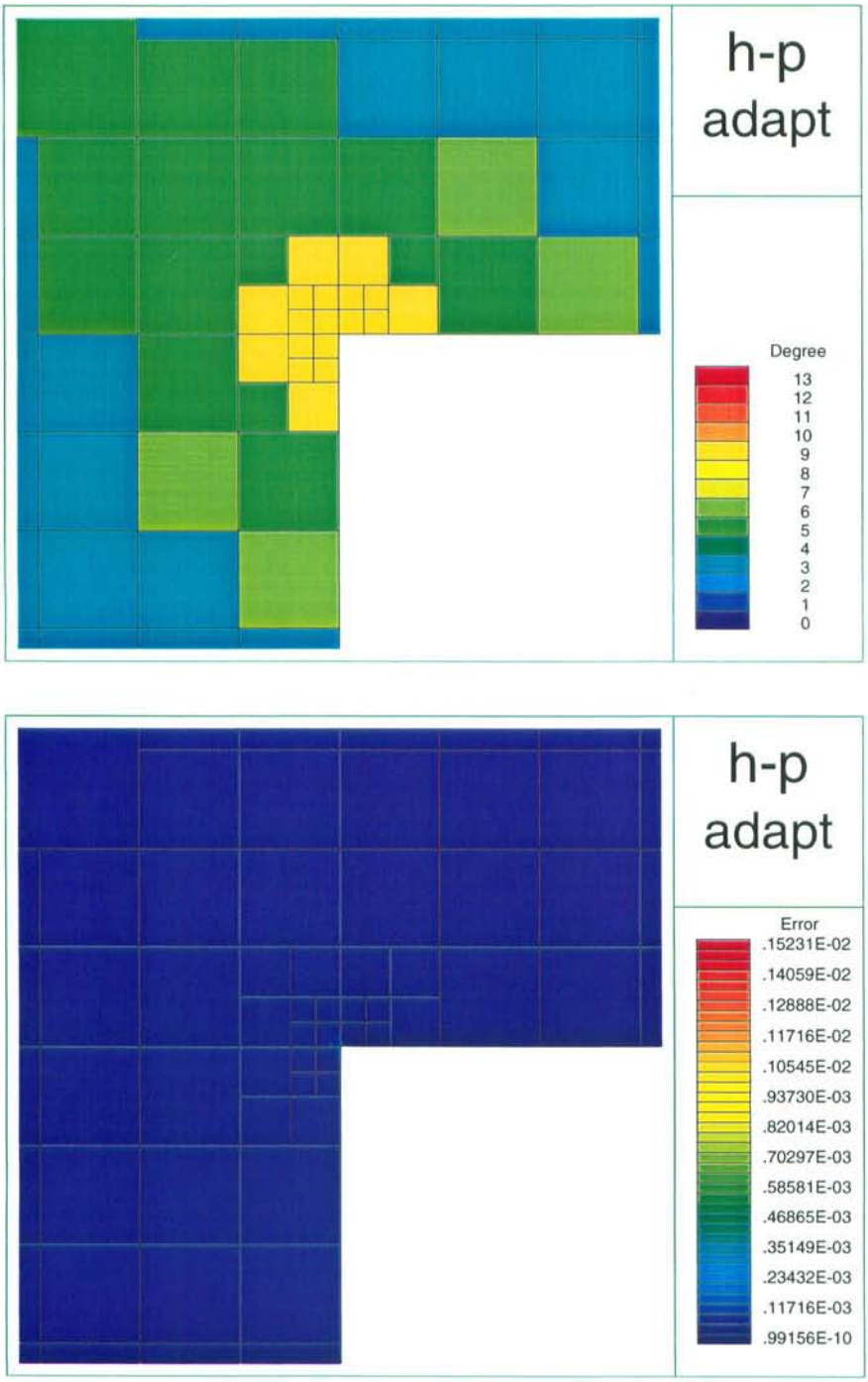

Figure 14: Stability test: ($\times 20$ at the corner) Top: $p-$enrichment at the singularity, Bottom: Pointwise error and mesh.

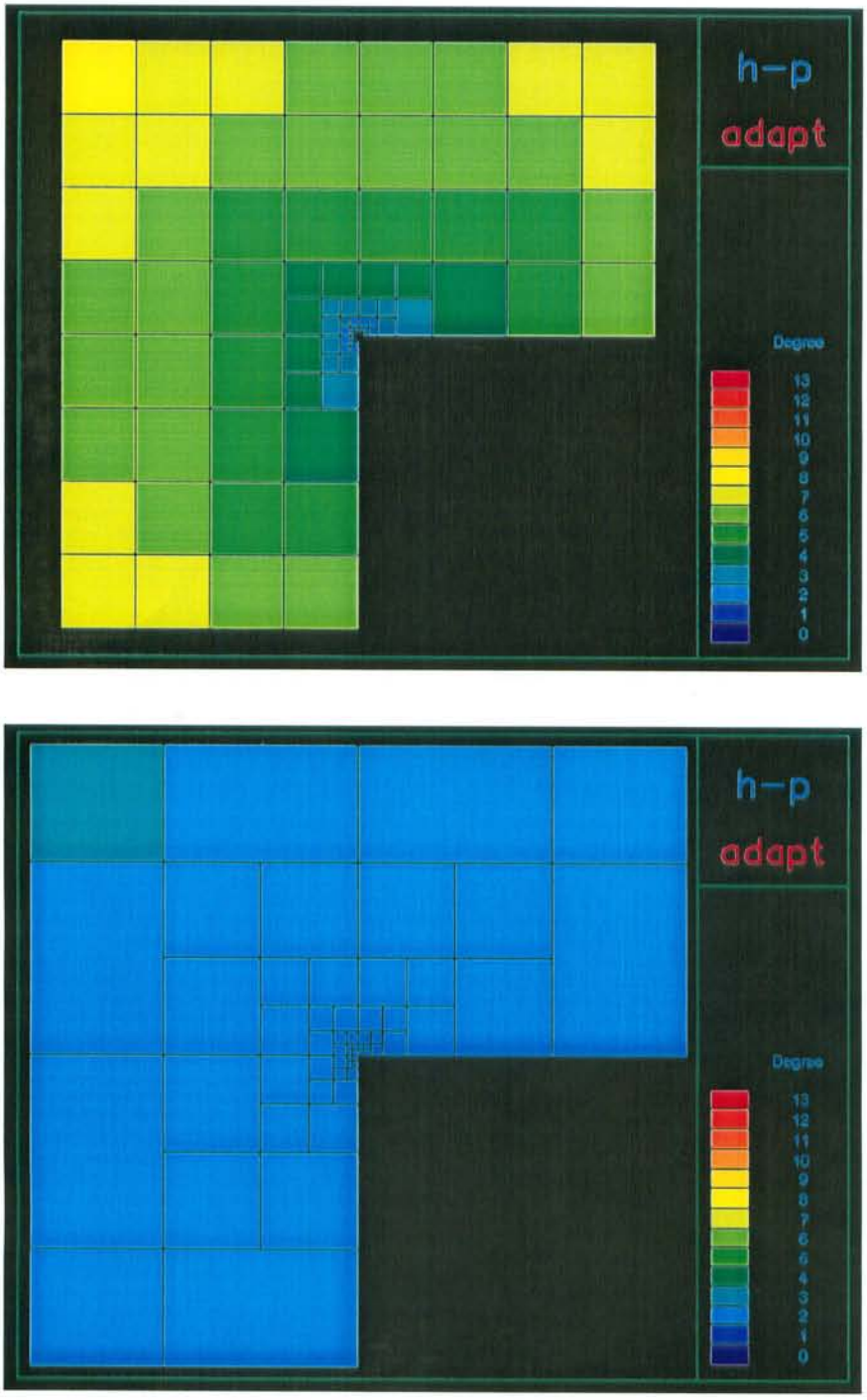

Figure 15: Top: Mesh and monomial basis after h-p adaptation, Bottom: $\times 20$ at the corner.

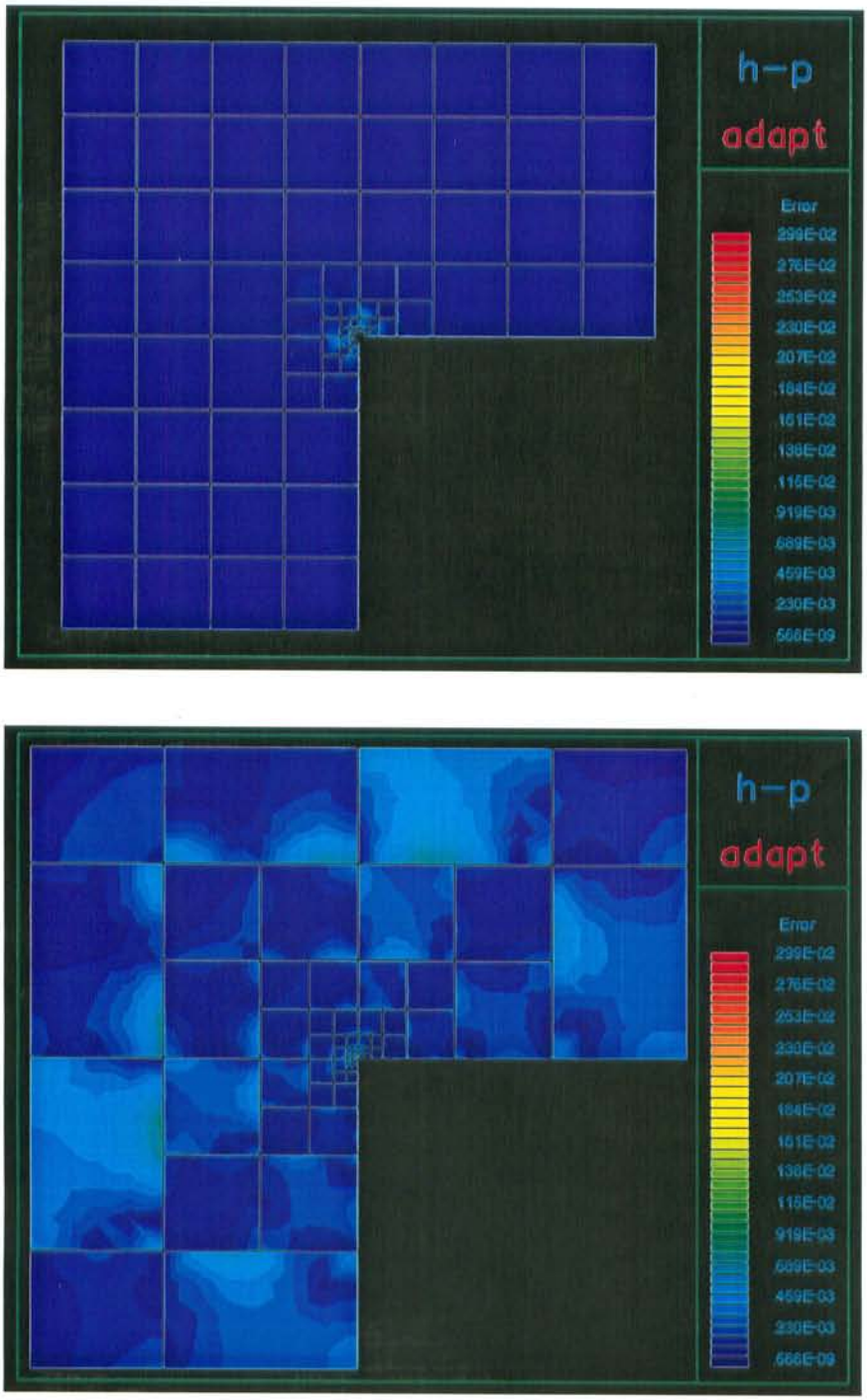

Figure 16: Top: Pointwise error, Bottom: $\times 20$ at the corner.

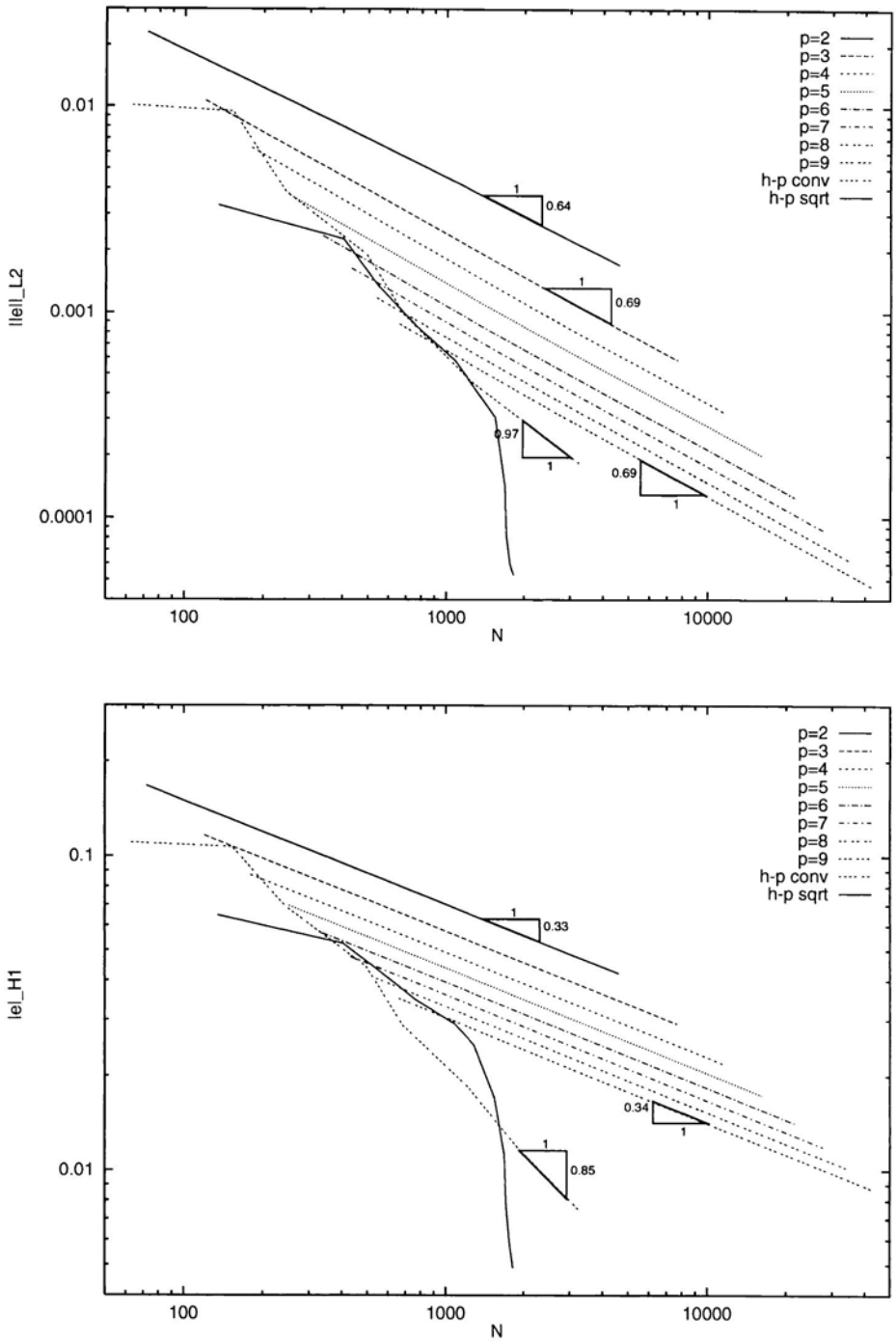

Figure 17: L-Shape domain: Convergence rates using global and adaptive refinements. Top: L^2 norm, Bottom: H^1 seminorm.